



**Feasibility Study of Perovskite Solar Cell Recycling**

**Md. Shahariar Chowdhury**

**A Thesis Submitted in Fulfillment of the Requirements for the Degree of  
Master of Science in Sustainable Energy Management  
Prince of Songkla University**

**2019**

**Copyright of Prince of Songkla University**



## **Feasibility Study of Perovskite Solar Cell Recycling**

**Md. Shahariar Chowdhury**

**A Thesis Submitted in Fulfillment of the Requirements for the Degree of  
Master of Science in Sustainable Energy Management  
Prince of Songkla University**

**2019**

**Copyright of Prince of Songkla University**

**Thesis Title**            Feasibility Study of Perovskite Solar Cell Recycling  
**Author**                    Mr. Md. Shahariar Chowdhury  
**Major Program**        Sustainable Energy Management

---

**Major Advisor:**

**Examining Committee:**

.....  
 (Dr. Narissara Nuthammachot)

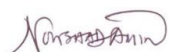
.....Chairperson  
 (Dr. Montri Suklueng)

**Co-advisor:**

.....Committee  
 (Dr. Narissara Nuthammachot)

.....  
 (Asst. Prof. Dr. Kuaanan Techato)

.....Committee  
 (Asst. Prof. Dr. Kuaanan Techato)



.....  
 (Prof. Dr. Nowshad Amin)

.....Committee  
 (Dr. wattana Ratismith)

.....Committee  
 ( Dr. Jiraporn Chomanee)

The Graduate School, Prince of Songkla University, has approved this thesis as fulfillment of the requirements for the Master of Science Degree in Sustainable Energy Management.

.....  
 (Prof. Dr. Damrongsak Faroongsarng)  
 Dean of Graduate School

This is to certify that the work here submitted is the result of the candidate's own investigations. Due acknowledgment has been made of any assistance received.

.....Signature

(Dr. Narissara Nuthammachot)

Major Advisor

.....Signature

(Mr. Md. Shahariar Chowdhury)

Candidate

I hereby certify that this work has not been accepted in substance for any degree and is not being currently submitted in candidature for any degree.

.....Signature

(Mr. Md. Shahariar Chowdhury)

Candidate

<b>Thesis Title</b>	Feasibility Study of Perovskite Solar Cell Recycling
<b>Author</b>	Mr. Md. Shahariar Chowdhury
<b>Major Program</b>	Sustainable Energy Management
<b>Academic Year</b>	2018

### ABSTRACT

Perovskite solar cells dependent on  $\text{CH}_3\text{NH}_3\text{PbI}_3$  and related materials have achieved great efficiencies, on a lab-scale. Nevertheless, subsequently these solar cells contain poisonous lead, a feasible system for management with the cells after their operational lifetime is essential to prevent performance of environment to lead and to conform to international electronic waste disposal guidelines. The aim of this research is to simulate of planar structure of perovskite solar cell, to fabricate the perovskite solar cell, to recycle the perovskites solar cell and to recovery the hazardous material lead and Fluorine doped Tin Oxide (FTO) substrate. First, Solar Cell Capacitance Simulator-1D (SCAPS-1D) was used to study the absorber layer defect density and n/i interface of perovskite solar cells versus various cell thickness values. The planar p-i-n structure was defined as PEDOT:PSS/Perovskite/CdS, and its performance was simulated. Power conversion efficiency  $>25\%$  can be achieved at  $<10^{15} \text{ cm}^{-3}$  defect density and  $>400 \text{ nm}$  thickness of absorber layer, respectively. The study assumed 0.6 eV Gaussian defect energy level below the perovskite's conduction band with a characteristic energy of 0.1 eV. These conditions resulted in an identical outcome on the n/i interface. Secondly, fabricated the planar structure(p-i-n) by using chemical deposition; where Au/Spiro-OMeTAD/perovskite/ $\text{TiO}_2$ /FTO/glass. However, PCE,  $V_{oc}$ ,  $J_{sc}$  and FF, 4.7%, 0.71 V,  $12.79 \text{ mA/cm}^2$  and 0.5 % respectively. According to the recycled process to eliminate every layer of the solar cells separately, which provides the opportunity to selectively the separate materials. Further separation of the toxic lead iodide in elevated revenue, it was seen that the  $\text{PbI}_2$  quantitatively and FTO substrate recovered for making new solar cell. In addition, further research can develop aqua regia solution method.

**Keywords:** Perovskite solar cell, PV waste, Mathematical simulation, Device fabrication, Perovskite solar cell recycle .

## ACKNOWLEDGEMENT

My deepest gratitude goes to Allah Almighty Who has provided all that was needed to complete this project and the program for which it was undertaken.

I offer my wholehearted gratitude and appreciation to my supervisors Dr. Narissara Nuthammachot, Asst. Prof. Dr. Kuaanan Techato and Prof. Dr. Nowshad Amin for their guidance and content support through in this research.

I am grateful to Assoc. Prof. Dr. Md. Akhtaruzzaman, Assoc. Prof. Dr. Chin-Hua Chia for their laboratory support.

Special thank goes to UKM & UNITEN research group in Malaysia, NARA Institute of Science and Technology in Japan for their laboratory support.

Thanks to Miss Paweenrat Na Phatthalung (FEM, PSU academic officer) and Ms. Sutawan Sathianwiriya (Bell) (FEM, PSU Public Relations Officer) for their excellent suggestions and guidance with essential academic and immigration processes respectively.

I am thankful to all my lab friends/learning partners especially Mahmudul Hasan, Dr. Kazi Sajedur Rahman, Mohamad Shah Jamal, Dr. Vidhya, Arif Billah and Md. Hafiz All Amin.

Finally, a big thanks to the Graduate School of PSU for the financial support to this thesis under a grant of Thai Education Hub (TEH-AC) scholarship.

Md. Shahariar Chowdhury

## TABLE OF CONTENTS

ABSTRACT.....	v
ACKNOWLEDGEMENT.....	vi
LIST OF FIGURES.....	viii
LIST OF TABLES.....	x
LIST OF ABBREVIATIONS AND SYMBOLS.....	xi
Chapter 1.....	1
Introduction.....	1
1.1. Renewable Energy:.....	1
1.2. Solar Photovoltaic Energy:.....	3
1.3. Perovskite solar cell:.....	5
1.4. Problem statement:.....	9
1.5. Research objective:.....	9
1.6. Research scope:.....	9
1.7. Organization of Thesis:.....	10
Chapter 2.....	11
Literature Review.....	11
2.1. The history of PV installations.....	11
2.2. Global photovoltaic shear market and waste generation.....	13
2.3. Causes of solar PV panel failure.....	16
2.4. Existing methods of the recycling process.....	17
2.4.1. Recycling process.....	17
2.4.2. Physical separation.....	18
2.4.3. Thermal and chemical treatment:.....	18
2.5. Recycling approaches.....	23
2.6. Social and environmental advantages.....	25
Chapter 3.....	27
Materials and Methods.....	27
3.1. Device simulation.....	27
3.2. Solar cell preparation.....	29
3.3. Solar cell recycling methodology:.....	30



3.3.1. Layer by layer:.....	30
3.3.2. One step solution:.....	32
3.4. Device characterization:.....	34
Chapter 4.....	35
Result and Discussion.....	35
4.1. Simulation result.....	35
4.1.1. Effect of absorber layer defect on different thickness:.....	35
4.1.2. Effect of defect on ETL interface CdS/perovskite absorber layer with thickness.....	39
4.2. Performance of perovskite solar cell:.....	41
4.3. Recycle characters layer by layer:.....	42
4.3.1. Trace Pb and Spiro-OMeTAD by UV-vis spectroscopy:.....	43
4.3.2. Qualitative of Spiro-OMeTAD.....	45
4.3.3. Quantitative analysis by ICP-MS measurement:.....	46
4.3.4. Qualitive and quantitative analysis for recycled FTO substrate:.....	47
4.3.5. Recycled FTO electrical properties by Hall effect measurement.....	50
4.3.6. FTO morphology and roughness analysis by AFM:.....	50
4.4. Qualitatively analysis of gold by XRD measurement.....	51
4.5. Recovered ITO substrate qualitative analysis by UV-vis spectroscopy:.....	52
4.6. Quantitative analysis by ICP-MS measurement:.....	53
4.7. Lab scal recycle cost :.....	54
Chapter 5.....	55
Conclusion and References.....	55
Conclusion.....	55
References.....	57
VITAE.....	66

## LIST OF FIGURES

Figure 1. 1 Growth in renewable electricity generation by region technology.....	1
Figure 1. 2 Growth in renewable electricity generation by region.....	2
Figure 1. 3 Power generating capacity installed in 2017.....	4
Figure 1. 4 Solar photovoltaic generation technology.....	5
Figure 1. 5 Types of the perovskite solar cell structure.....	6
Figure 1. 6 Design of deep and shallow level defects in an energy band diagram. ....	8
Figure 2. 1 Global growth of solar PV capacity.....	11
Figure 2. 2 The top 10 countries worldwide by total installed solar PV capacity at the end of 2017. ....	12
Figure 2. 3 Market share of PV panels by technology type (2014-2030).....	14
Figure 2. 4 Failure rates according to customer Complaints. ....	17
Figure 2. 5 Different types of solar PV recycling processes.....	18
Figure 2. 6 PV wafers during heating procedure: (a) before heating; (b) after heating; (c) the reverse side before heating and (d) reverse of side after heating. ....	19
Figure 2. 7 The estimated cumulative worldwide solar PV module waste (tons) 2016- 2050. ....	26
Figure 3. 1 Schematic perovskite tool construction and Energy level chart.....	28
Figure 3. 2 Perovskite solar cell preparation: a) glass substrate ready for TiO <sub>2</sub> deposition. b) With my supervisor during the deposition time. c) our research group Spin coating deposition. d) after PbI <sub>2</sub> deposition. e) deposition electrode. f) during the annealing solar cell on hotplate. g) Finally made full cell. h) Me and my research group.....	30
Figure 3. 3 Layer by layer recycle process of the planar structure of perovskite solar cell. ....	31
Figure 3. 4 (a) Perovskite solar cell for prepared recycle. (b) Selected the best cell for recycle. (c) removal of the gold and Spiro-OMeTAD layer. (d) After remove the cell electrode and HTM layer prepare for absorber layer recycle. (e) After recycled the FTO coated glass substrate (f) Storage the liquid solution. ....	31
Figure 3. 5 One step aqua regia chemical bath process. ....	33

Figure 3. 6 One step recycle process: a) Prepared aqua regia solution. b) solar cell chemical bath into the jar recovered ITO glass substrate. d) storage used chemical for analysis. ....	33
Figure 4. 1 Outline displays of perovskite solar cell show limitations colony on absorber defect density and thickness. ....	38
Figure 4. 2 Outline displays of perovskite solar cell show limitations colony on defect density of CdS/perovskite interface and perovskite's thickness. ....	40
Figure 4. 3 JV characteristics of the planar structure perovskite solar cell. ....	42
Figure 4. 4 a) SEM micrograph cross-sectional of the full cell device. b) Top view of the full cell. c) Cross-section of the fresh FTO coated glass. d) Top view of fresh FTO coated glass. e) cross-section of recycled FTO coated glass. f) Top view of recycled FTO coated glass. ....	42
Figure 4. 5 UV-Vis absorption spectra of (a) DMF containing extracted lead iodide and (b) reference solution of commercial lead iodide dissolved in DMF. ....	43
Figure 4. 6 Chlorobenzene including obtained Spiro-OMeTAD. ....	44
Figure 4. 7 H-NMR spectroscopy of recycled Spiro-OMeTAD and DMSO-d6 pick. ....	45
Figure 4. 8 H bond of Spiro-OMeTAD recycled powder. ....	46
Figure 4. 9 TiO <sub>2</sub> after the removing PbI <sub>2</sub> . ....	47
Figure4. 10 X-ray deflection (XRD) analysis: a) Fresh FTO glass substrate b) Recycled FTO glass substrate. ....	48
Figure 4. 11 Energy-dispersive X-ray spectroscopy (EDX), a) Element percentage of fresh FTO substrate b) element percentage of recycled FTO substrate. ....	49
Figure 4. 12 Transmittance spectra of fresh FTO and recycled FTO substrate. ....	49
Figure 4. 13 AFM 3D top surface (a) Fresh FTO substrate (b) Recycled FTO substrate. ....	51
Figure 4. 14 XRD analysis for recycled gold. ....	52
Figure 4. 15 Transmittance spectra of Fresh ITO and recycle ITO substrate. ....	53

## LIST OF TABLES

Table 2. 1 Year of PV installations and waste generation. ....	15
Table 2. 2 Silicon based solar photovoltaic module recycling methods advantage and disadvantage.....	21
Table 2. 3 Thin film solar photovoltaic modules recycling methods advantage and disadvantage.....	21
Silicon based solar photovoltaic module recycling methods .....	21
Table 2. 2 Thine film solar photovoltaic modules recycling methods. ....	21
Table 3. 1 List of parameters used in this mathematical simulation .....	29
Table 4. 1 Metal concentrations measured by ICP-MS.....	47
Table 4. 2 Electrical properties of fresh FTO and recycled FTO.....	50
Table 4. 3 AFM roughness data. ....	51
Table 4. 4 Metal concentration measured by ICP-MS .....	53

## LIST OF ABBREVIATIONS AND SYMBOLS

RETs	: Renewable energy technologies.
TWh	: Terawatt-hour.
GHG	: Greenhouse Gas.
EU	: European Union.
IEA	: International Energy Agency.
SDS	: Sustainable Development Scenario.
PV	: photovoltaic.
CO <sub>2</sub>	: Carbon dioxide.
KWh	: Kilowatt hour.
WEEE	: Waste Energy & Electronic Equipment.
PSCs	: Perovskite solar cells.
GWh	: Gigawatt hour.
a-Si	: Amorphous silicon.
CdTe	: Cadmium telluride Copper indium gallium diselenide (CIGS).
CIS	: Copper indium diselenide.
HTM	: Hole Transport Material.
ETL	: Electron transport layer.
NiO <sub>x</sub>	: Nickel Oxide.
CuI	: Cuprous Iodide.
Spiro-OMeTAD	: 2,2',7,7'-tetrakis(N,N'-di-p-methoxyphenylamine)-9,9' Spirobifluorene.
PEDOT: PSS	: Poly(3,4-ethylenedioxythiophene):Poly(styrenesulfonate).
TiO <sub>2</sub>	: titanium dioxide.
ZnO	: Zinc Oxide.
SnO <sub>2</sub>	: Tin Oxide.
Zn <sub>2</sub> SnO <sub>4</sub>	: Zinc stannate.
DLTS	: Deep level transient spectroscopy.
MAI	: methylammonium lead iodide.

FTO	: Fluorine doped tin oxide.
ITO	: Indium doped Tin Oxide.
EoL	: End-of-life.
Pb	: lead.
Cd	: cadmium.
EVA	: ethylene vinyl acetate.
PCBM	: [6,6]-Phenyl-C61-Butyric Acid Methyl Ester.
PSC	: Perovskite Solar Cell.
p-i-n	: Inverted Planar.
CH <sub>3</sub> NH <sub>3</sub> PbI <sub>3</sub>	: Methylammonium lead iodide.
CH <sub>2</sub> Cl <sub>2</sub>	: Dichloromethane.
CuSCN	: Copper(I) thiocyanate.
DMF	: Dimethylformamide.
DMSO	: Dimethyl sulfoxide.
DSSC	: Dye Sensitized Solar Cell.
TFSCs	: Thin film solar cells.
CdS	: cadmium sulfide.
Au	: Gold.
UV-Vis	: Ultraviolet–visible spectroscopy.
EDX	: Energy-dispersive X-ray spectroscopy.
SEM	: Scanning electron microscope.
FESEM	: Field Emission Scanning Electron Microscopy.
NMR	: Nuclear magnetic resonance spectroscopy.
ICP-MS	: Inductively coupled plasma mass spectrometry.
XRD	: X-ray diffraction.

## Chapter 1

### Introduction

#### 1.1. Renewable Energy:

Renewable energy technologies (RETs) have settled advantages including I) improving environmental sustainability, ii) improving public health iii) creating job and iv) financial benefit [1]. Renewables expanded by 4% in 2018, representing about one-fourth of worldwide energy development. The power division drove renewables-based power to expand at its quickest pace this decade. Solar photovoltaic (PV), hydropower, and wind each represented about 33% of the development, with bioenergy representing a large portion of the rest [2]. Renewables secured practically 45% of the world's power development, presently representing over 25% of worldwide power yield. In 2018, solar PV energy created around 136 TWh of power, which expanded by 30% from 2017. Wind and hydropower energy expanded by 29% to 132 and 129 TWh, respectively, from 2017 to 2018. Other renewable energies contributed about 12% (52 TWh) in 2018 [3].

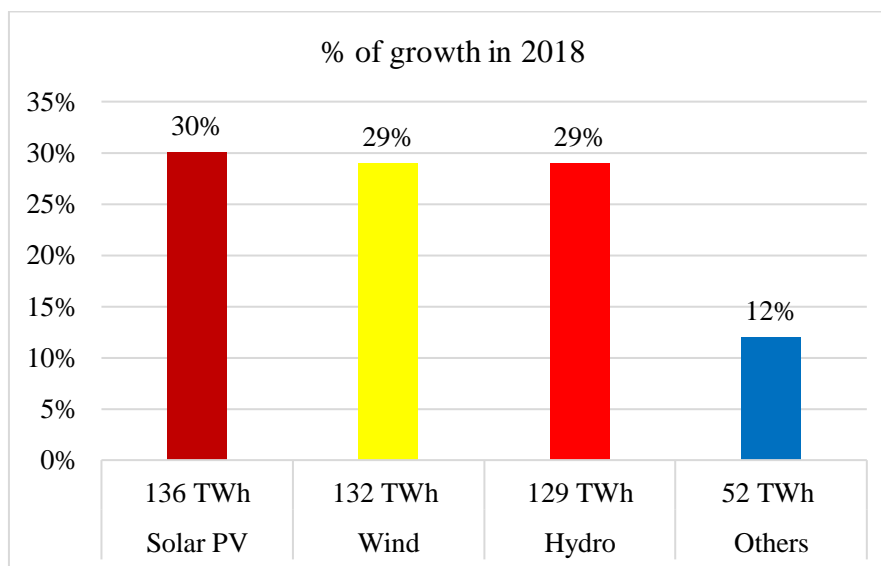


Figure 1. 1 Growth in renewable electricity generation by region technology, 2017-18 [3].

China represented over 40% of the development in renewable-based power, trailed by Europe, which represented 25%. The United States and India jointly contributed another 13% [3]. Renewables have quickly developed outside of these

significant markets. In consideration of the environmental impacts of greenhouse gas (GHG) emissions, organizations of renewable energy technologies receive high incentives for motivation [1]. Renewable resources, such as solar power and wind control, have received tremendous aid for advancement.

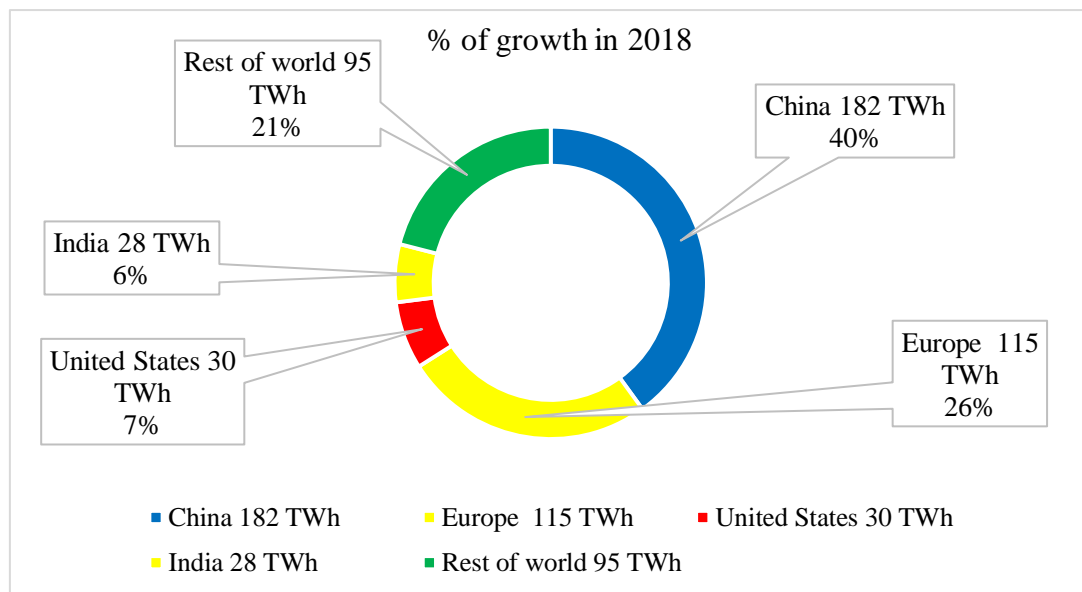


Figure 1. 2 Growth in renewable electricity generation by region , 2017-18 [3].

The EU's unique Renewable energy order (2009/28/EC) sets a coupling focus of 20% last energy utilization from renewable sources by 2020. To accomplish this, EU nations have focused on achieving their own national renewable focuses for 2020, running from 10% in Malta to 49% in Sweden. Each of these nations is required to have at least 10% of their vehicle powers originate from renewable sources by 2020. In December 2018, the new updated Renewables energy order (2018/2001) established another coupling renewable energy focus (i.e., 32%) for the EU in 2030, with a statement for a conceivable upward modification by 2023 [4]. In general, the utilization of renewables needs to grow considerably more rapidly in every one of the three segments to be on track to meet long-haul atmosphere objectives, cleaner air goals, and give access to present-day energy sources, as shown in the IEA Sustainable Development Scenario. In this situation, the portion of renewables in the power blend needs to ascend from one-quarter today to 66% in 2040. In the arrangement of warmth, renewables need to ascend from 10% today to 25%. In a vehicle, renewables need to



ascend from 3.5% today to 19%, including both immediate and backhanded use, for example, renewable power for warming and electric vehicles [4]. Renewable energy assets are normally rechargeable, and a portion of the assets is unending, such as solar energy.

## **1.2. Solar Photovoltaic Energy:**

Solar photovoltaic (PV) power technologies, which were first applied in space, can now be used everywhere that electricity is required and has many different applications. In addition to being easy to fit and use, PV technology is eco-friendly and has become a popular means of generating power and solar energy technology and is currently the third most-used renewable energy source in the world after hydro and wind power which occupy the first and second positions, respectively [5]. Moreover, PV energy sources generate power with low levels of carbon emissions which cause global warming [6]. In addition, Fossil fuel-generated electricity accounts for CO<sub>2</sub> (Carbon dioxide) emissions of between 400 and 1000g CO<sub>2</sub> eq/kWh (Kilowatt hour) whereas CO<sub>2</sub> emissions from silicon-based solar panels are negligible [7].

Solar power has many advantages as a source of renewable energy. It is safe, reliable and profitable and can easily be shared, and PV technology is a very exciting prospect as a way of fulfilling the world's future energy needs. During the last decade, the use of solar PV panels has increased, and there is now a large global market for PV panels which have the potential to produce clean energy globally. Moreover, it is expected that during the present century, PV-generated electricity will become the primary global energy source [8]. 2017 was an especially notable year for the solar PV sector, with the level of solar PV generating capacity installed globally rivalling that of other energy production technologies. In fact, solar power added more new capacity than was added to both nuclear and fossil fuel energy-generation capacity (Figure 1.3) and the installed capacity of solar and wind power technology almost doubled, with an additional 99.1 GWh (Gigawatt hour) of solar PV energy becoming grid-connected in 2017 [9].

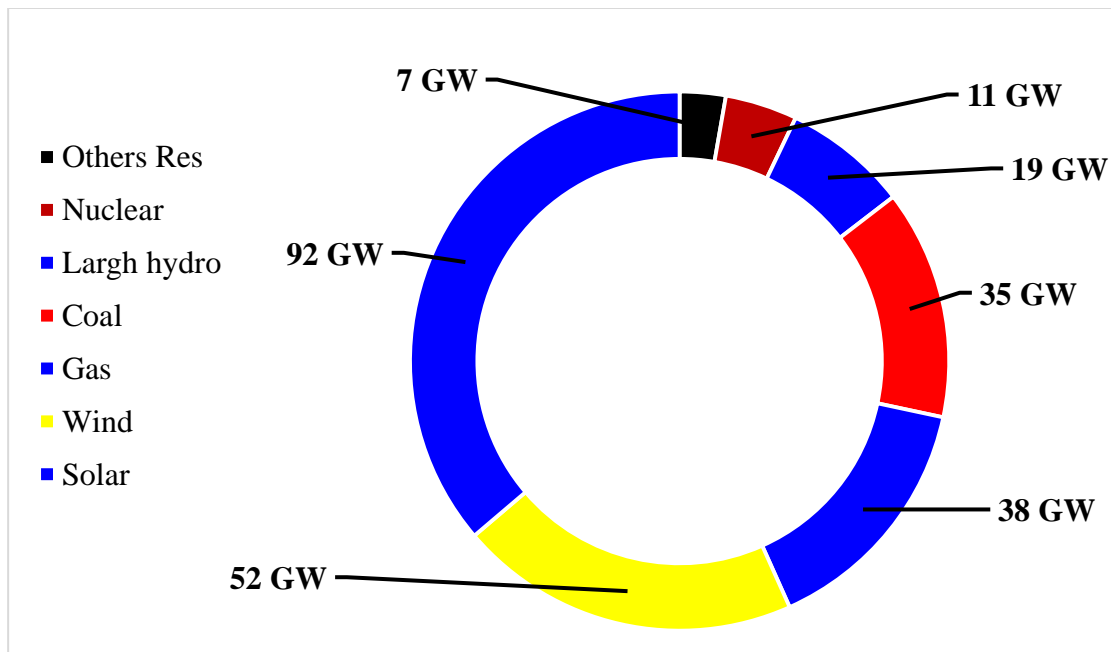


Figure 1. 3 Power generating capacity installed in 2017 [10, 11].

Large-area solar PV installations help to reduce development costs. Saudi Arabia put out tenders for a 300MW plant in February 2018 which will produce solar energy at the world's lowest price of 0.0234 USD/kWh [11] and world solar energy prices have reduced rapidly because of developments in solar technologically. China led the world in solar power production in 2017 and in that year, for the first time it installed 50 % of the world's new solar power generating capacity [10]. On the other hand, in the same year Europe had a slower rate of increase in its solar generation capacity, which grew by only 30 % compared to the previous year. Nevertheless, by the end of 2022, global solar energy generation capacity may grow to as much as 1270.5 GW and solar-generated power 2022 will therefore exceed one terawatt (TWh) [11].

The European commission's Waste Energy & Electronic Equipment (WEEE) directive, 2012/19/UE was passed by the European parliament and came into force on 13 August 2012 and became effective on 14 February 2014, and this is now applicable to the management of waste solar panels, both household and industrial, in Europe. The natural resources used in manufacturing solar PV panels qualify as auxiliary raw materials within the applicable regulations [12]. However, PV waste must be properly disposed of and treated, and in Europe, the export of waste is prohibited. Quite apart from the economic, environmental and social implications of this

prohibition, it promotes the recycling of solar PV components [5]. There are numerous kinds of solar cells, however, over 80% of them that are at present created overall comprise of crystalline silicon cells [13]. The second most utilized semiconductor material is cadmium telluride, which empowers the generation of slender film cells. The scope of current advances and conceivable future choices is assembled as recorded beneath:

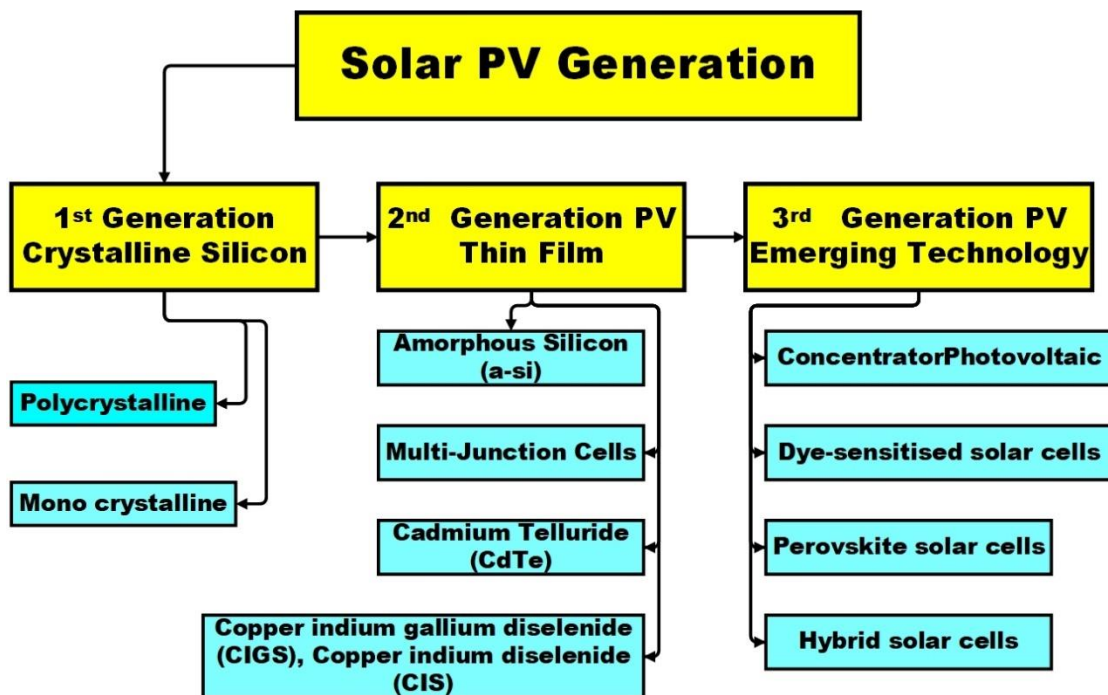


Figure 1. 4 Solar photovoltaic generation technology [5].

### 1.3. Perovskite solar cell:

Hybrid inorganic–organic PSCs have attracted considerable attention in the PV business because of their high productivity, low-temperature preparation, and simple manufacture procedure. Hybrid inorganic–organic perovskites demonstrate high ingestion coefficients, high charge-bearer versatility, low exciton restricting energy, long exciton dispersion length, and an effectively tunable bandgap. In 2009, Miyasaka first demonstrated PSCs. The  $ABX_3$  perovskite structure is building an essential development square of the natural inorganic PSC. It is the least complex structure for creating  $BX_6$  octahedra, where B is a metal cation and X is the anion together with the best possible charge to quality the A and B cations (where  $A > B$ ) [1, 2]. The A cations

seal the massive 12-overlap synchronized openings among the octahedra. In general, the  $BX_6$  octahedra point dispersal by the A ions in the cuboctahedral interstices is characterized by a perovskite structure and a cubic  $Pm\bar{3}m$  precious stone structure [3]. Similar to previously reported unit organometal halide perovskites, 'A' is a natural or inorganic cation (i.e.,  $MA^+$ ,  $FA^+$ ,  $Cs^+$ ,  $Rb^+$ , and  $K^+$ ), 'B' is a metal cation in perovskite (i.e.,  $Sn^{2+}$  or  $Pb^{2+}$ ), and 'X' is a halide anion (i.e.,  $Cl^-$ ,  $Br^-$ , and  $I^-$ ) [4]. Primarily,  $ABX_3$ -XYZ type half-breed organometal includes different halide perovskites, such as  $MAPbI_{3-x}Cl_x$  and  $MAPbI_{3-x}Br_x$ , which have attracted considerable attention because of their high tunable optical properties [5,4]. In 2009, Kojima gathering was the first run through to presented natural inorganic PSC, the color sharpened solar cells organized among the  $CH_3NH_3PbI_3$  and  $CH_3NH_3PbBr$  the relating effectiveness depended on of 3.13% and 3.81% for  $MAPbI_3$  and  $MAPbI_3$  solar cells [1]. The  $CH_3NH_3PbI_3$  structure accomplished up to 9.7% effectiveness in 2011. Lee et al.(2013) utilized the blended halide perovskite component  $CH_3NH_3PbI_{3-x}Cl_x$  as a safeguard and electron transporter and obtained up to 10.9% productivity [6]. A mass heterojunction with a confined HTM needs to be developed. The Chinese Academy of Sciences ensured by National Renewable Energy Laboratory obtained the highest effectiveness of 23.3% to date. The PSC has three types of device structure: planar, inverted planar, and mesoporous.

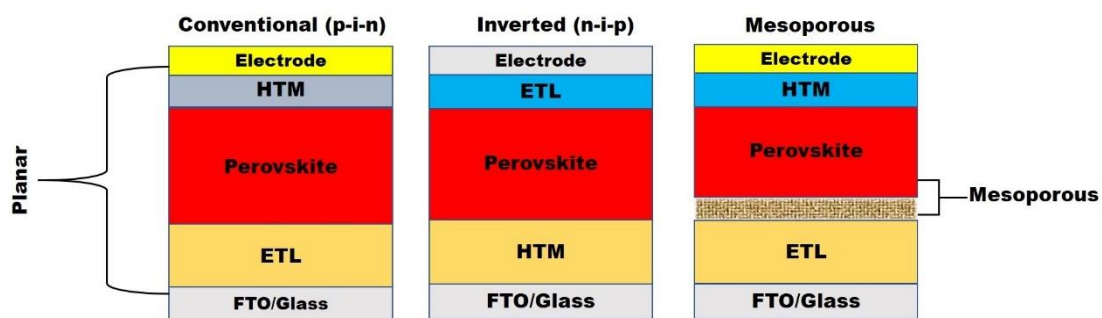


Figure 1. 5 Types of the Perovskite solar cell structure [21].

A mesoporous PSC contains a packed electron transport layer (ETL) and a mesoporous film inside the perovskite safeguard for proficient electron transportation. However, planar-organized perovskite technologies are highly anticipated for wide applications. Normally, planar PSCs (P-PSCs) are made-up with a comparative working key as slender film solar cell innovation. P-type semiconductors, such as  $NiO_x$ ,

CuI, and Spiro-OMeTAD, have been utilized as an opening vehicle layer in PSCs. Marios Neophytou et al. [8] found that PEDOT:PSS as a gap transport layer can increase proficiency by 13%. In P-PSC, numerous n-type semiconductor materials have been connected to ETL. For example, TiO<sub>2</sub>, ZnO, SnO<sub>2</sub>, and Zn<sub>2</sub>SnO<sub>4</sub> have been utilized as an ETL in the typical structure of PSCs [7]. These materials require high temperature toughening for wide applications.

These materials are limited by phase isolation under illumination due to halide relocation Hoke's effect, which leads to a high open-circuit voltage ( $V_{oc}$ ) deficit (>500 meV) and consequently causing photostability [18]. Investigations on perovskite solar cells focus on the improvement of power conversion efficiency through careful application of new deposition techniques to engineer morphological properties and compositional fine-tuning of perovskite layers. Different Si-based cells fabricated through a well-controlled semiconducting method, whereas perovskite solar cells are produced via a solution-based method [23]. These methods produce a number of defects during manufacture, which are the fundamental factors that influence productivity and reproducibility. Mid-gap states in a band structure are formed and partake in bearer recombination. The managing trap structure and intensity are significant for achieving reproducible outcomes with high efficiency. Thus, solar-oriented perovskite cells can be built by applying one-step and two-step techniques and may be analysed by deep level transient spectroscopy (DLTS) [17].

Yin et al (2019) determined the transition-state energies of all known characteristic point trap in methylammonium lead iodide structures using standards [17]. They discovered that both shallow- and deep-level defects exist within the bandgap. Similar defects were observed in other studies. Approximately  $10^{10}$ – $10^{11}$  cm<sup>-3</sup> are identified as shallow defects with significantly large charge-limited current measurements, whereas deep level defects are identified to have  $10^{14}$ – $10^{16}$  cm<sup>-3</sup> with time resolved photoluminescence, transient photocurrent measurements and deep level transient spectroscopy [17, 24]. Seo et al. stated that the one-step solar cell has considerably more defects than the two-step deposited perovskite solar cell [17]. The efficiency of MAPbI<sub>3</sub> solar-powered cells is limited by the presence of defective conditions that decrease mobility, increase transporter recombination and cause electrical destabilisation [25]. The defect was characterized as either shallow or deep,

as shown in Figure 1.6 Shallow defects, which are inside a couple of thermal energy items of a band point, do not impede productivity much, as they normally catch just one kind of bearer, which is discharged rapidly. Deep defects are situated close to the focal point of the bandgap and become increasingly inconvenient, because they catch the two kinds of bearers, which can be moderately avoided, thereby permitting enough time for charge transporter recombination [16].

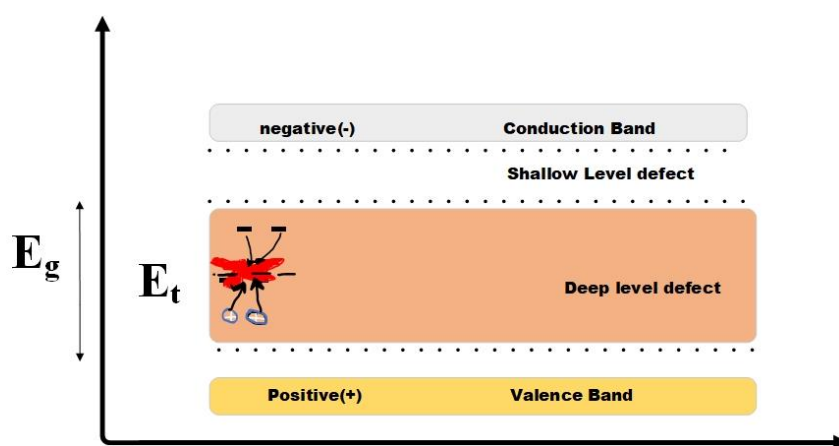


Figure 1. 6 Design of deep and shallow level defects in an energy band diagram.

Structure and defect density cases change the physical and electrical properties of ionic crystals [26, 27]. Moreover, the deformities are frequently involved in transport, which decide the property of materials' highly significant functionalities, such as diffusion barriers and oxygen particle conductors. Formation of strong oxide film or scale occurs when metals react with oxygen. Despite decay on metals, defects (e.g. vacancies, interstitial atoms, dislocations and grain boundaries) improve the feedback method by offering a route for fast oxygen diffusion or a positive spot for the outcome to occur [28]. Based on oxidation conditions (e.g. temperature, time, weight and gas arrangement), the reaction may have varying microstructures and morphologies that can create micro-cracks or microchannels. Arrangement and gathering of deformities on oxide and their impact on oxidation have been observed. Confined consumption that causes erosion is considered a very significant destabilising component influencing the position of materials [18, 29].

#### **1.4. Problem statement:**

PSCs can achieve high power conversion efficiency within a short time. But are not yet available in the market, as their commercial availability would require clear strategies for recycling and disposal. Due to the presence of lead, which is a hazardous heavy metal, that causes environmental and human health issues. Secondly, the electrodes of PSC are usually made of gold or silver, while the transparent conductive oxide is manufactured from fluorine-doped tin oxide (FTO) or indium tin oxide (ITO) which are expensive raw materials resulting in high prices for the panels.

#### **1.5. Research objective:**

To execute the stated problems stated, three research objectives have been formulated from the research areas mentioned in the problem statement. The research objectives of this study are as follows:

1. To simulate the planar structure of the PSC for selection of a suitable parameter for making the device.
2. To observe cell stability and efficiency by fabricating the planar structure of the PSC device.
3. To recycle the planar structure of the PSC device through chemical treatment.
4. To obtain the recovery material and FTO glass substrate.

#### **1.6. Research scope:**

The first aim of this study was to find the most suitable parameters of the PSC structure through SCAPS-1D software simulation. Through the simulation thickness of layers was investigated to identify the suitable thickness for device fabrication, the defect density of PSCs was also clarified, and the number of materials per square meter were measured. The second aim of this study was to synthesize the planar structure of the PSC in order to investigate its efficiency and stability. The last aim of this study was to recycle the PSCs using layer-by-layer separation method. Through this recycling process the amount of re-useable materials like electrodes (gold) etc. were measured and their quality for re-use was also investigated.

### 1.7. Organization of Thesis:

**Chapter 1** is an overview of global renewable energy generation, various renewable resources of energy generation with focus on solar energy and its potential, and solar photovoltaic generation. It also lists the key points of PSC, the problem statement of perovskite recycles, and three research objectives to solve continuing issues regarding this technology. A short conversation of the thesis association is also provided.

**Chapter 2** provides an overview of the photovoltaic recycling history. The first part of this chapter discusses the installation of solar PV energy. The second part explains in brief the generation of solar waste and the causes of PV failure. The final part of this chapter describes the different types of solar PV recycling.

**Chapter 3** describes the materials and methods used for developing PSCs. The first part of this chapter highlights the simulation method used for the planar structure of perovskite. The second part of this chapter contains the solution preparation methods used in the device fabrication. The third part of the chapter explains in detail the two recycling processes.

**Chapter 4** contains the conclusions drawn from the works described in this thesis. The results obtained from this research are presented chronologically according to the objectives.

**Chapter 5** the final part of this chapter summarizes the characterization tools and techniques used for all the experimentations performed in this thesis. The future prospects of this work are also enumerated.



## Chapter 2

### Literature Review

#### 2.1. The history of PV installations:

There are various types of solar PV cells, but nowadays the c-Si solar cell dominates over 80 % of the market globally [5]. These thin film solar cells are second generation, semi-conductor-controlled solar cells made from materials such as cadmium telluride (CdTe). In 2017, the total newly installed capacity was 99.1 GW globally, which was approximately the same as the total installed up until the end of 2012 (100.9 GW) [5]. By the end of 2017, the total installed capacity exceeded 400 GW, with the figures in 2015-2016 rising from around 200 GW to 300 GW [4]. The cumulative installed solar-power capacity increased by 32 % between 2016 and 2017 from 306.4 to 404.5 GW as can be seen from Figure 2.1 [3]. In 2007 Germany was the first country to sanction the commercial connection of solar power to their national grid, at which time they commenced a tariff scheme [10]. Between 2007, when the installed global capacity was 9.2 GW, and the end of 2017 the cumulative installed capacity had increased by around 43% [4].

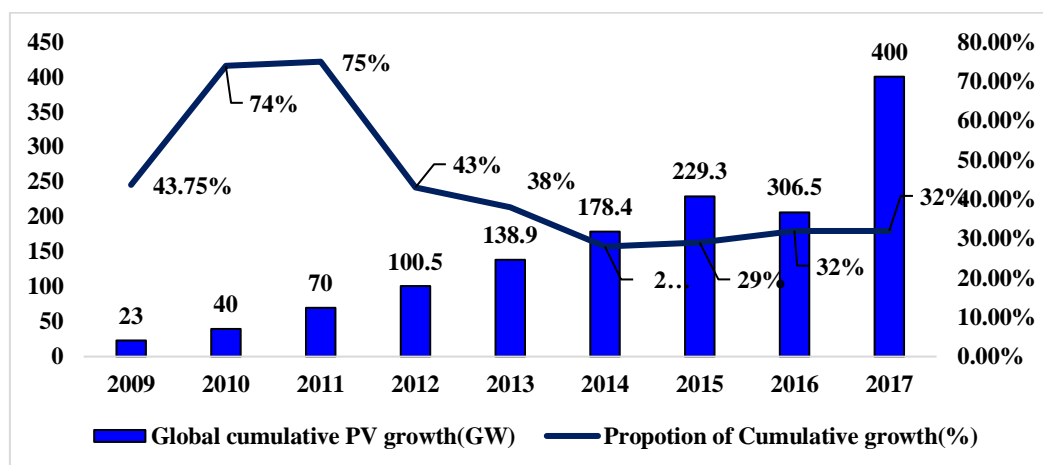


Figure 2. 1 Global growth of solar PV capacity [4, 11, 29, 30].

In 2017 the Asia-Pacific region had become the leading area for solar power having increased its capacity over 2016 by 73.7 GW to reach a total installed capacity of 221.3 GW, which represents a 55 % share of global capacity (see Figure 2.1) [10]. Whilst European nations were the solar-power pioneers and still together

occupy second position in the world capacity ranking, based on a cumulative PV capacity of 114 GW, their share has slipped to 28% [6]. The United State of America are in third position with a total installed capacity of 59.2 GW, or 15% [8]. The share of Africa and the Middle East reduced in 2017, and even after adding 2.1 GW, the total solar capacity of 6.9 GW represented only 1.7 % of global capacity [6]. Almost one third (32.3 %) of the world's solar power generation capacity is operated by China (see Figure. 2.2), based on a substantial increase from the 2016 [4]. China for the first time became the world's largest solar power generating nation in 2017, having increased its share from around 25 % in the previous year followed by Japan [4]. The United States, and in 2017, the United States overtook Japan although the share of the total world capacity of both countries was reduced [31].

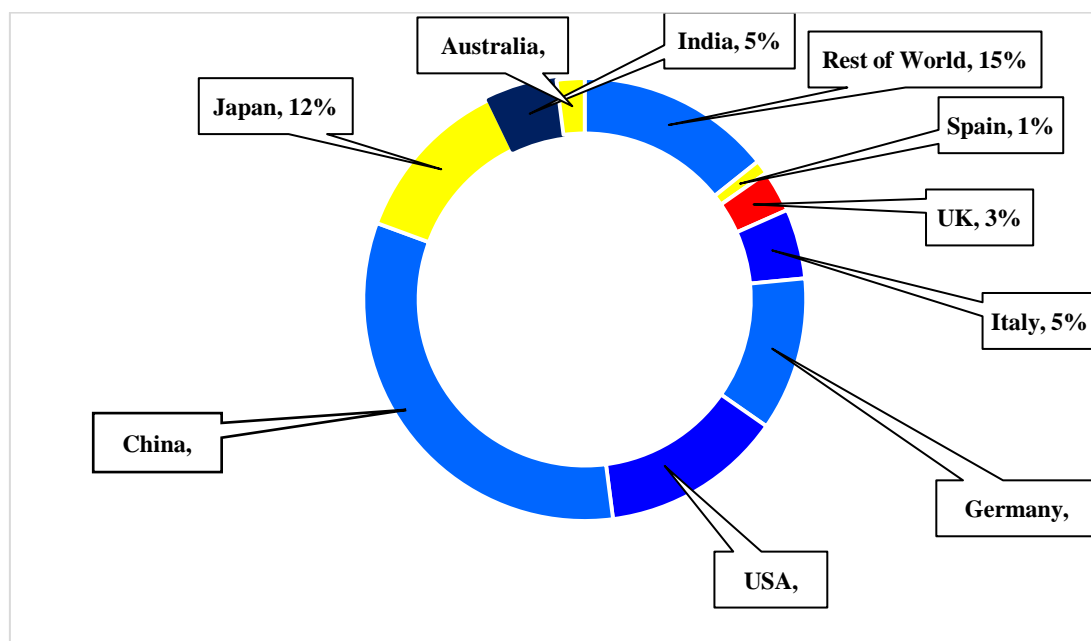


Figure 2. 2 The top 10 countries worldwide by total installed solar PV capacity at the end of 2017 [31].

Based on their share of worldwide capacity, Japan's 49.3 GW reduced to 12.2 % in 2017, compared to 13.8 % in 2016, and none of the European nations individually were among the top three solar power generating nations [3]. Only Germany, which had the fourth largest capacity achieving a double-digit global share, due to a low 2017 new-installation figure of 1.8 GW which resulted in a drop-in global share to 10.6 %, from 13.4 % in 2016 [4]. Further, for the first time in 2017, India was

among the top five countries, having added more than 10 GW of solar generation capacity to increase its share of global installed capacity to 4.7 %, and doubling its total PV capacity in 2017 to 19 GW [4]. At the end of 2017, the United Kingdom and Italy were the only other two countries with more than 10 GW of installed solar capacity, with Italy at 19.4 GW and the United Kingdom at 12.7 GW [3]. Based on current estimates it is unlikely that in 2018, any other countries will increase their installed capacities to 10 GW with Australia (7.3 GW), France (8 GW) and Spain (5.6 GW) some way below that level in 2017 [31].

## **2.2. Global photovoltaic shear market and waste generation:**

The market share of solar panels by technology group is shown in Figure 5. Currently, the volume of comprehensive connected PV panels is rising sharply, and rapid growth is expected in the coming years, since the typical useful life of a solar panel is 25 years [12]. However, it is expected that the total quantity of end-of-life (EoL) PV panels will reach 9.57 million tons by 2050 [8]. In 2014 the market was dominated by silicon based. c-Si panels, which accounted for a 92 % share of the market with those based on CdTe technology at 5 % and those on copper indium gallium (di)selenide (CIGS), 2 %, with 1 % accounted for by those manufactured from other materials (dye-sensitized, CPV, organic hybrids) [8]. The market share of c-Si PV panels is expected to decrease from 92 % to 44.8 % between 2014 and 2030, while that of third-generation PV panels has been rising rapidly, and is predicted to reach 44.1 %, from a base of 1 % in 2014, over the same period [8, 12, 29-31].

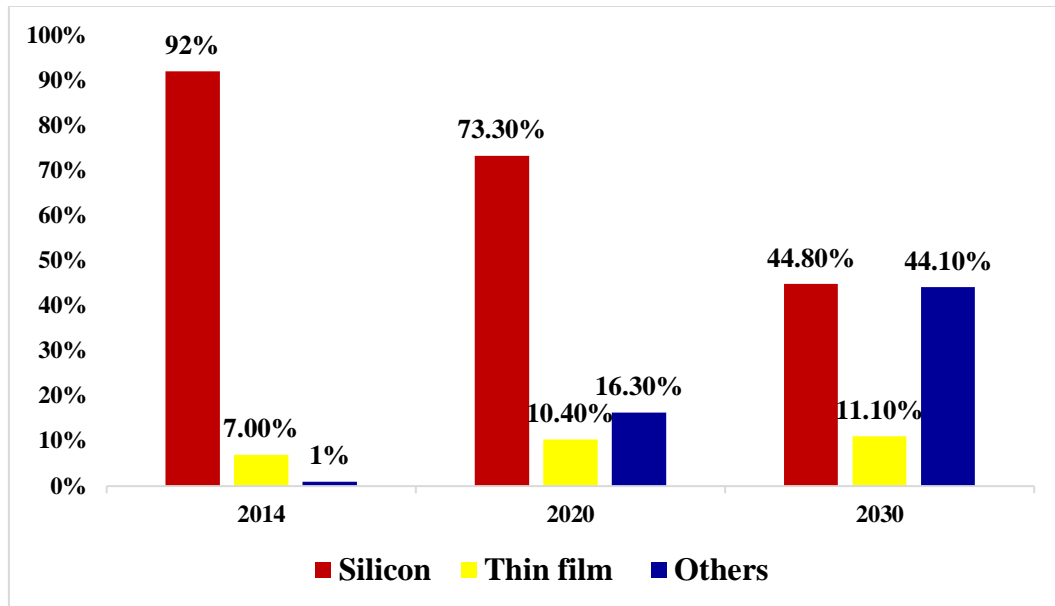


Figure 2. 3 Market share of PV panels by technology type (2014-2030) [30,31].

Solar photovoltaic panels lose efficiency over time probably, whose allowed to operate life is 20 to 30 years at least [5]. The International Renewable Energy Agency estimated that at the end of 2016 there are around 250,000 metric tons of solar panel waste in the world [30]. Solar panels contain the lead (Pb), cadmium (Cd) and many other harmful chemicals that couldn't be removed only if the entire panel is cracked [30]. The Environment Minister in Japan advised in November 2016 that Japan's production of solar panel waste each year is expected to rise from 10,000 to 800,000 tons by 2040 and that the country has no plans to dispose of them safely and effectively [12]. A recent statement found that the reprocessing of all solar massive waste Japan bent by 2020 would take Toshiba Environmental Solutions 19 years [30]. The yearly waste making is 70 - 80 times higher by 2034 than the year before 2020 [31]. China has a larger number of solar plants, currently operates around two times as many solar panels as the USA and has no proposals to the dumping of the whole old panels. In China, the Eiffel Tower's weight could also be 20 million metric tons or 2000 times as extremely high as 2050 [31]. Despite the presence of environmental awareness, California, another world leader in solar panels, has also no waste disposal plan. At the end of their useful lives, only Europe requires the production of solar panels to collect and dumping solar waste. Although solar panels were disposed of on regular sites, it is

not advised because modules can degrade and harmful chemicals can leach into the ground, causing drinking water major issues.

The lifetime of PV modules has been estimated in 25 years, on Average; so, it can be assumed that the installed PV power (MW) becomes waste after that period. To identify the time shifting, Table 2.1. shows the years of installation (x) and the years of waste generation(y), so  $y = x + 25$  [5].

Table 2. 1 Year of PV installations and waste generation [5].

<b>Year of Installations (x)</b>	<b>Years of waste generations (y)</b>
<b>y=x+25</b>	
1987	2012
1992	2017
1997	2022
1998	2023
1999	2024
2000	2025
2001	2026
2002	2027
2003	2028
2004	2029
2005	2030
2006	2031
2007	2032
2008	2033
2009	2034
2010	2035
2011	2036
2012	2037
2013	2038
2014	2039
2015	2040
2016	2041
2017	2042
2018	2043
2019	2044
2020	2045
2021	2046
2022	2047
2023	2048
2024	2049
2025	2050

Currently, two types of PV recycling technology are commercially available but other technologies are also under research. Panels manufactured using c-Si technology occupy the major market share with thin film technology using either CdTe or CIGS technology as the second largest market sector [5]. The recycling processes for c-Si PV panels are different from those applied to thin film PV panels because of their different module structures. One important distinction is that the target of disposing of the encapsulant from the layered structure of compound PV modules is to recover both the quilted glass and the substrate glass that contains the semiconductor layer.

Therefore, the aim for c-Si modules is to divide the c-Si glass and to recover the Si cells, and other metals. The method used in recycling Si-based PV panels is to separate the layers, which entails removing the encapsulant from the panel and the Si cells to recover the metals. The removal of the encapsulant from the laminated structure is not straightforward and many possible approaches exist, including thermal, mechanical, and chemical. Chemical methods recapture metals from Si cells, by, for instance, etching and other processes. The substrate glass and the metals in the semiconductors are separated and recovered and the metals can then be isolated and purified. [29, 30].

Most waste is typically generated during four primary life cycle phases of any given PV panel. These are 1) panel production 2) panel transportation 3) panel installation and use, and 4) end-of-life disposal of the panel [30]. The following waste forecast model covers all life cycle stages except production. This is because it is assumed that production waste is easily managed, collected and treated by waste treatment contractors or manufacturers themselves and thus not a societal waste management issue.

### **2.3. Causes of solar PV panel failure:**

There are relatively few defects found in new solar panels, with light erosion (0.5 % - 5 %) and poor design and defects arising during manufacture being the main causes [32]. Other causes of panel failure have been claimed to be due to electrical equipment, such as junction boxes, fuse boxes, charge controllers and cabling as well as issues with grounding. In the early years of their production, solar panels suffered

from degradation of the anti-reflective coating layer of colourless ethylene vinyl acetate (EVA) applied onto the glass, as well as incoherency due to cracked solar cells. During their first 12 years of use, failures were caused by repeated load cycles due, for instance to wind or snow, as well as temperature changes which caused degradation, contact defects in junction boxes, glass breakage, burst frames, breakage of cell interconnections and problems with the diodes associated with a higher rate of degradation of cells and interconnectors [32]. Previous research has shown that 40 % of PV panel failures are due to microscopic cracks, and failures from this cause have been most common in newer panels manufactured after 2008 when production of thin-cell panels began [32].

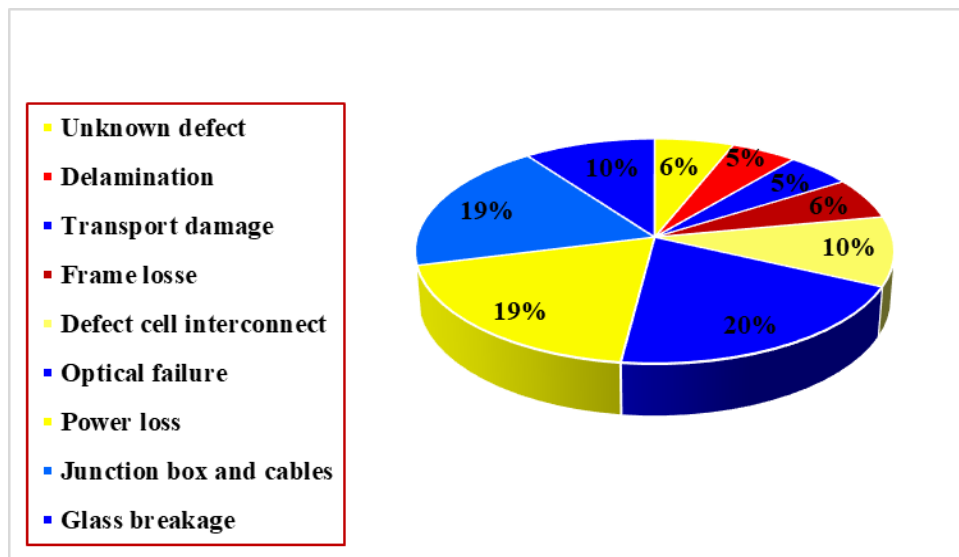


Figure 2. 4 Failure rates according to customer Complaints [32].

## 2.4. Existing methods of the recycling process:

### 2.4.1. Recycling Process:

Nowadays, Japan, Europe and the US are focused on solar module recycling research and development [33, 34]. Most efforts related to solar-panel recycling concentrate on Si panels and aim to recover and recycle the most important parts. As stated above, there are presently three different types of recycling process applied to solar PV panels, physical, thermal and chemical as illustrated in Figure 2.5 [8].

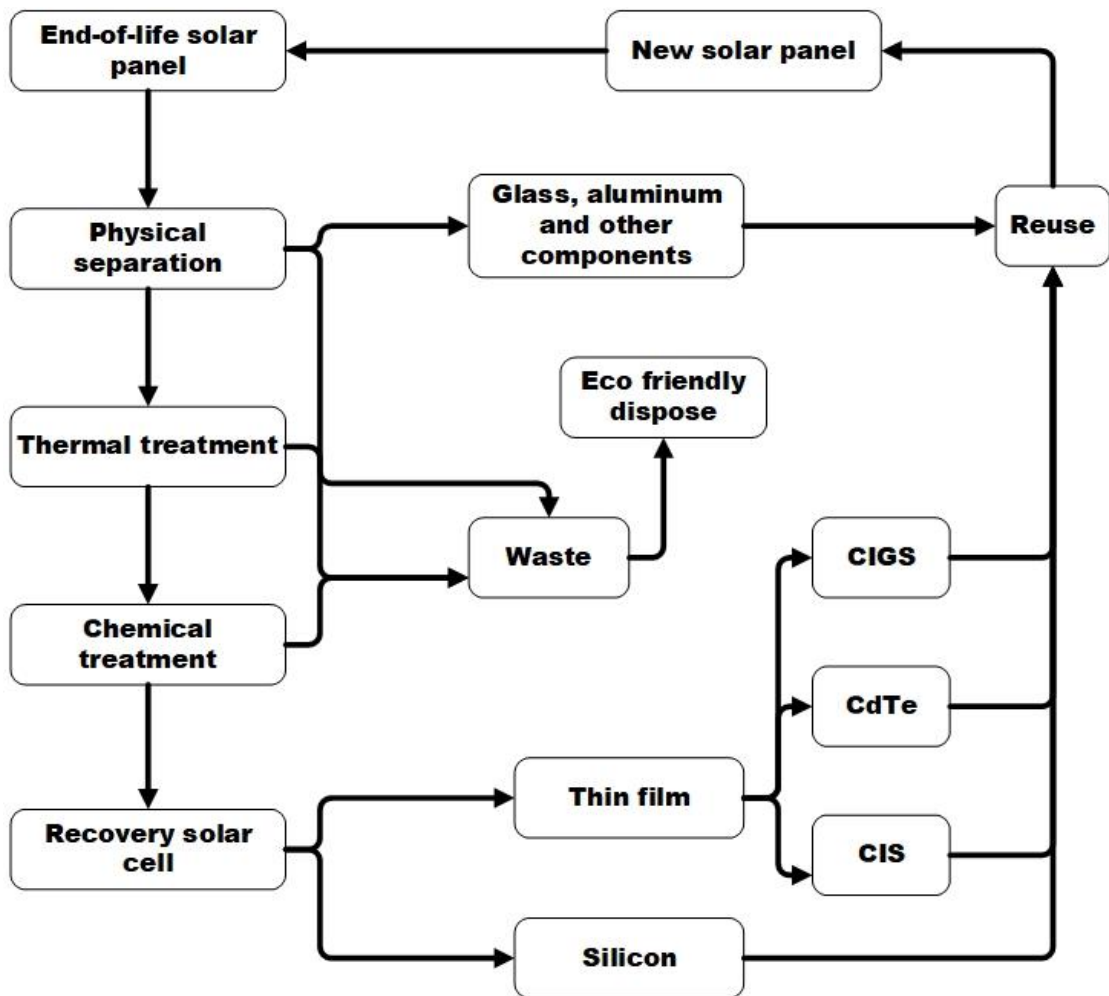


Figure 2. 5 Different types of solar PV recycling processes [35, 36].

#### 2.4.2. Physical Separation:

The replacement of elements in solar cells in order to repair systems is confined to replacing electrical components and does not include material separation or cell treatment [37]. There are two widely used types of process to check for and repair junction box faults and repairing such faults can help to increase the output power of older solar panels. However, this method can only be used for external junction boxes located outside of the main body of the solar panel.

#### 2.4.3. Thermal and chemical treatment:

Pagnanelli et al. [38] used mechanical crushing to reduce the glass to a size of  $>1$  mm and further crushing was able to recover different grades of the glass



fraction, all of which were <1 mm, on which thermal treatment, with an air flux of 30 l/h was then applied to recover the glass and metal fractions. The heating rate was gradually increased until it reached 650 °C at a rate of 10 °C/min and the furnace was then maintained at that temperature for 1 hour. An overall glass recovery rate of 91 % was achieved by this means. Meanwhile, Orac et al. [37] used thermal pretreatment followed by acid leaching to recover copper and tin from used circuit boards.

Shin, Park and Park [7] recycled 60 multi-crystalline Si wafers (156 mm×156 mm) which had been manufactured in South Korea by JSPV Co. Ltd. Thermal treatment was first applied to separate the layers of the solar panels [35, 39] as shown in Figure 2.6. The thermal treatment was conducted in a K-Tech. Co (South Korea) furnace. (1500 mm wide x 1700 mm high x 2000 mm long). The wafers were first coated with a phosphoric acid paste and then heated for periods of 2 min at five temperatures ranging from 320 to 400 °C. The resulting recovered wafers were successfully used in manufacturing solar panels and the efficiency of the cells was found to be similar to that of the original product.

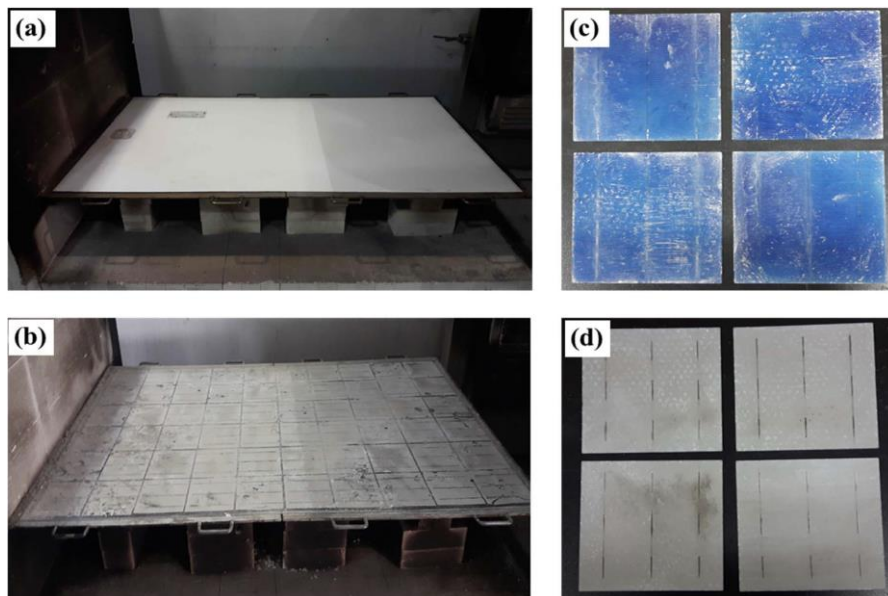


Figure 2. 6 PV wafers during heating procedure: (a) before heating; (b) after heating; (c) the back side before heating and (d) back of side after heating [7].

Doi et al. [33] applied various organic solvents to crystalline-silicon solar panels to remove the EVA layer, which was found to be melted by diverse types

of organic solvents, of which trichloroethylene was found to be the most effective. The solar panels (125 mm x 125 mm) were treated in a process, using mechanical pressure, which was essential to suppress the swelling of the EVA during soaking in trichloroethylene for ten days at 80 °C. The reclaimed Si panels were able to be used efficiently after the recycling process.

Kim and Lee et al. [40] reported enhancing the rate of EVA layer dissolution by using different types of organic solvents (trichloroethylene, O-dichlorobenzene, benzene, toluene etc.) aided by an ultrasonic process. The research tested combinations of different solvents, temperatures, ultrasonic power and radiation times. After one hour, the EVA layer was fully dissolved in 3 mol/L of toluene at a temperature of 70 °C with exposure to ultrasound at a power of 450 W. However, a problem noted with this process was that lead resulted as a hazardous by-product.

Marwede et al. [41] reviewed the available means of treating EoL PV materials and noted that the pH value changed during three periods when sodium hydroxide was used for metal recovery [42]. In other work, 5N Plus recovered metals by evaporation in a thickening tank and the metals were recovered by filtering during dewatering. First Solar to whom 5N Plus supply metals, announced a recovery rate for Cd and Te of 95- 97 % [43] with both metals then being capable of being reused in First Solar products [44].

Wang and Fthenakis et al. [45] conducted Cd and Te separation by using various ion-exchange resins on the metals in a sulphuric acid solution over different time periods [46-48]. The recovered metals were eluted from their ion-exchange/acid solutions, and high recovery rates above 90 % were recorded. In another study, the recovery of Te from solution was noted to be accelerated by the use of sodium carbonate and sodium sulphide.

Dattilo et al. [49] reported the wet-chemical extraction of metals from CIGS panels. The method relied on deselenizing the composites, recovering the Cu and separating other metals such as In and Ga. The CIGS materials were directly decomposed by electrolysis with the Cu and Se settling onto the cathode and the metals deposited the cathode plate were then removed and separated by oxidization and distillation to produce Cu, Se with ZnO and InO being compounded by exhalation.

Table 2. 2 Silicon based solar photovoltaic module recycling methods advantage and disadvantage.

Technology	Process	Advantages	Disadvantages	Ref.
Delamination	Physical breakup	<ul style="list-style-type: none"> <li>➤ Efficient of handling waste.</li> </ul>	<ul style="list-style-type: none"> <li>➤ Other materials mixed with EVA .</li> <li>➤ Damage of solar cells.</li> <li>➤ Apparatus decomposition.</li> </ul>	[3,43, 44]
	Thinner dissolution (Organic Chemistry)	<ul style="list-style-type: none"> <li>➤ Organic layer removed from glass.</li> <li>➤ Waste chemical reusable.</li> <li>➤ Simple removal of EVA.</li> </ul>	<ul style="list-style-type: none"> <li>➤ Time necessary for delamination depends on area.</li> <li>➤ Expensive equipment.</li> <li>➤ Hazardous for human health.</li> </ul>	[18, 38]
	Nitric acid dissolution	<ul style="list-style-type: none"> <li>➤ EVA and metal layer fully removed from the wafer.</li> <li>➤ Possible recovery of the whole cell</li> </ul>	<ul style="list-style-type: none"> <li>➤ Dangerous emissions.</li> <li>➤ Cell defects due to inorganic acid.</li> </ul>	[48]
	Thermal treatment	<ul style="list-style-type: none"> <li>➤ EVA fully eliminated.</li> <li>➤ By reusing wafers, possible to regain whole cell</li> </ul>	<ul style="list-style-type: none"> <li>➤ Involves high energy consumption.</li> <li>➤ Dangerous emissions</li> </ul>	[32, 41 42]
	Ultrasonic irradiation	<ul style="list-style-type: none"> <li>➤ Used as a supplementary process to accelerate dissolution process</li> <li>➤ Simplifies removal of EVA.</li> </ul>	<ul style="list-style-type: none"> <li>➤ Very costly process.</li> <li>➤ Waste solution treatment.</li> </ul>	[26]
Material Separation	Dry and wet mechanical process	<ul style="list-style-type: none"> <li>➤ Non-chemical process.</li> <li>➤ Simple process.</li> <li>➤ Requires low energy.</li> <li>➤ Equipment widely available.</li> </ul>	<ul style="list-style-type: none"> <li>➤ No removal of dissolved solids</li> </ul>	[30]
	Etching	<ul style="list-style-type: none"> <li>➤ Uncomplicated but effective process.</li> <li>➤ Recovery of high purity materials</li> </ul>	<ul style="list-style-type: none"> <li>➤ High energy demand because of high temperatures needed.</li> <li>➤ Use of chemical.</li> </ul>	[39]

Table 2. 3 Thin film solar photovoltaic modules recycling methods advantage and disadvantage.

Technology	Process	Advantages	Disadvantages	Ref.
Delamination	Physical breakup	<ul style="list-style-type: none"> <li>➤ Feasible to obtain various wastes by treatment (Split modules, submodules and laminated modules).</li> </ul>	<ul style="list-style-type: none"> <li>➤ Mixing of the various material fractions. Results in a loss from each material fraction.</li> <li>➤ Glass still partly combined with the EVA.</li> <li>➤ Breakage of solar cells so not possible to use them again.</li> </ul>	[4, 43, 44]
	Thinner dissolution (Organic Chemistry)	<ul style="list-style-type: none"> <li>➤ Organic layer removed from glass.</li> <li>➤ Reprocessing solutions.</li> <li>➤ Simple removal of EVA.</li> </ul>	<ul style="list-style-type: none"> <li>➤ Time necessary for delamination depends on area.</li> <li>➤ Cannot be dissolved fully and EVA still adheres to glass surface.</li> </ul>	[18, 38]

	Thermal treatment	<ul style="list-style-type: none"> <li>➤ EVA fully eliminated.</li> <li>➤ By reusing wafers, possible to regain whole cell.</li> </ul>	<ul style="list-style-type: none"> <li>➤ Involves high energy consumption.</li> <li>➤ Dangerous emissions.</li> </ul>	[32, 41,42]
	Radiotherapy	<ul style="list-style-type: none"> <li>➤ Easy to remove EVA</li> </ul>	<ul style="list-style-type: none"> <li>➤ Slow process</li> <li>➤ Very costly process.</li> </ul>	[32, 21]
Material Separation	Erosion	<ul style="list-style-type: none"> <li>➤ Does not need chemicals</li> <li>➤ Glass can be recovered</li> </ul>	<ul style="list-style-type: none"> <li>➤ Additional treatment pre-purification necessary</li> </ul>	[40]
	Vacuum blasting	<ul style="list-style-type: none"> <li>➤ Removal of semiconductor layer without chemical dissolution.</li> <li>➤ Glass can be recovered</li> </ul>	<ul style="list-style-type: none"> <li>➤ Emission of metallic fractions with abrasives.</li> <li>➤ Relatively long processing time.</li> </ul>	[27,44]
	Dry and wet mechanical process.	<ul style="list-style-type: none"> <li>➤ Non-chemical method.</li> <li>➤ Simple process.</li> <li>➤ Needs low energy.</li> <li>➤ Apparatus usually available.</li> </ul>	<ul style="list-style-type: none"> <li>➤ No removal of dissolved solids</li> </ul>	[30]
	Tenside chemistry	<ul style="list-style-type: none"> <li>➤ Tensides are reusable.</li> <li>➤ Metals fully removed from glass.</li> </ul>	<ul style="list-style-type: none"> <li>➤ Emulsions must be adapted to different cell technologies</li> <li>➤ Delamination time depends on the area.</li> </ul>	[41, 45]
	Leaching	<ul style="list-style-type: none"> <li>➤ Metal fully removed from glass.</li> <li>➤ Further extraction of metal solutions possible.</li> </ul>	<ul style="list-style-type: none"> <li>➤ Very high use of chemicals.</li> <li>➤ Control of the chemical reactions is complicated.</li> </ul>	[45,46]
	Flotation	<ul style="list-style-type: none"> <li>➤ Comparatively easy method.</li> <li>➤ Limited use of chemicals</li> </ul>	<ul style="list-style-type: none"> <li>➤ Material separated at various stages of flotation</li> <li>➤ Inadequate purity of materials separated.</li> </ul>	[40,44]
	Etching	<ul style="list-style-type: none"> <li>➤ Recovery of high purity materials.</li> <li>➤ Low cost but effective process</li> </ul>	<ul style="list-style-type: none"> <li>➤ High energy demand because of high temperatures needed.</li> <li>➤ Use of chemical.</li> </ul>	[39]
Material purification	Hydrometallurgical	<ul style="list-style-type: none"> <li>➤ Commercially applicable in short time.</li> <li>➤ Low and controllable emissions</li> <li>➤ Easy water management</li> </ul>	<ul style="list-style-type: none"> <li>➤ Many separation and absorption steps.</li> <li>➤ Chemical process steps must be adapted to respective technology.</li> </ul>	[32,40, 45]
	Pyrometallurgical	<ul style="list-style-type: none"> <li>➤ Established industrial process.</li> <li>➤ Feedstock can contain different materials .</li> </ul>	<ul style="list-style-type: none"> <li>➤ High throughput necessary.</li> <li>➤ Some materials are lost in slag.</li> <li>➤ Heavy metals or unwanted materials are produced</li> </ul>	[32,38, 40,45]

Table 2.2 & 2.3 summarizes the various solar-panel recycling technologies currently available. Whilst many of these methods have been the subject of laboratory-based research there are currently only two commercially available treatments. The US-based solar manufacturer First Solar applies both mechanical and chemical treatment methods to thin film solar panels. On the other hand, c-Si solar-panel modules have been recycled by a company in Germany [ 57].

China has limited facilities for recycling involving component repair and panel separation and hires technology from outside to conduct separation and recycling of individual materials. Similarly, other countries have problems in applying recycling technologies; for instance, physical or mechanical processes generate a huge amount of dust which contains glass and, is therefore toxic, and the processes are also a source of noise pollution. The separation of the EVA layer by inorganic solvents leads to the emission of nitrogen oxides and other harmful gases [58], and their inhalation constitutes a health risk. In addition, the process of reusing the silicon wafers involves frame removal and it is difficult to dispose of the remaining liquid. Further, the time required for EVA dissolution by familiar organic solvents is long but can be accelerated by using ultrasound. However, the process also produces a very large amount of organic-melted waste, which is difficult to treat. Thermal and chemical methods thus combine advanced technology but have the disadvantage that they produce toxic gases and consume high amounts of energy.

## **2.5. Recycling approaches:**

Within the European Union the first country to adopt the EU's WEEE directive relating to the disposal and recycling of solar PV materials was the UK, in which it became law in 2014, and the second EU country to ratify the directive was Germany which also now follows the WEEE regulations. Under the directive, all producers or importers of solar PV materials, including solar panels, have to register under a product consent scheme in which all data about the panels etc. must be provided by the manufacturers, and producers and importers have to accept responsibility for the EoL treatment of their products, or are subject to large fines. Moreover, the European Union and the Czech Republic have entered into a joint venture for the recycling and recovery of EoL solar PV panels following the WEEE directive. Worldwide the

recycling of PV products requires that producers employ waste management techniques themselves or employ the services of companies or non-profit organizations and solar PV waste management advisors to help them deal with the problem of EoL panels. Currently the Czech company, Retina offers itself as both a reprocessor and as an advisor in relation to reprocessing management. In Europe the WEEELABEX organization which operates out of the Czech Republic is responsible for the preparation of standards and the awarding of certification in respect of the collection, storage, processing, and reprocessing of WEEE and the monitoring of waste-processing companies.

Outside of Europe, a small number of countries have addressed the issue of solar panel waste regulations. In Japan, solar panel waste recycling is under the control of the Japanese environment ministry and solar panel manufacturers participate in research into recycling technology with local companies being involved in research relating to reprocessing technology in Europe. Moreover, the European PV organization and Shell Oil Company (Japan) have entered into an association and NPC, a solar-panel and equipment manufacturer, have entered into a joint venture with Hamada an industrial waste-processing company, to recycle solar panels, and in 2016, the two companies jointly founded a PV processing improvement project through the New Energy Industrial Technology Development Organization (NEDO).

In the USA, the state of California Department of Toxic Substances Control (DTSC) offered to take responsibility for solar waste treatment, when European facilities' capacity decreased and the DTSC has now increased its recycling capacity and upgraded their facilities for the disposal of hazardous items after treatment [9]. The USA-based solar panel manufacturing company, First Solar has established factories in the United States, Germany, and Malaysia, which also employ recycling methods with recovery rates of 95 % for Cd and 90 % for glass. It will not be long before China will become the world largest solar panel producer, but it does not yet have strong policies relating to recycling and even its environmental protection authority has not yet focused on waste recycling [59]. However, Both Yingli Solar and Trina Solar are studying solar PV development and recycling.

Different types of waste, particularly electronic waste, are coming to be regarded as a liability which should be managed by the manufacturer of the products of

which the waste is composed [30]. Making manufacturers liable for EoL PV panels would encourage sustainable management of PV materials [60,61]. Moreover, manufacturers should be encouraged to adopt eco-friendly designs by enforcing appropriate regulations, because this would help to cut down the environmental impact of PV products, which can also be aided by conserving resources through the collection and recycling of EoL products [63] as well as promoting the manufacture of new solar panels using recycled materials. Finally, strict laws should be passed relating to the collection and recycling process, which will help the creation of a logistical network to support the productive technology and to create links in the eco-supply chain.

## **2.6.Social and environmental advantages:**

At the end of 2016 various estimates of the volume of solar PV waste ranged between 43,000 and 250,000 tons worldwide and the comparatively small amount. Currently being produced renders reprocessing not economically viable the projected growth of waste PV panels up to 2050 with different projections based on regular and early loss scenarios [31]. Based on the increase in the installed PV generation capacity in the current decade, the number of EoL panels will necessitate a strategy for recycling and recovery. The worldwide ratio of solar PV waste to new installations is expected to increase considerably over time, as shown Figure 2.7 reaching between 4 to 14 % of total generating capacity in 2030 and rising to over 80 % (around 78 million ton) in 2050. Based on the literature analysing the expected rates of panel installation and EoL solar panels, most of those will be c-Si over the next several years [50], and thus methods of dealing with solar PV waste material, principally by recycling need to be in place by 2040. If that were done, by recycling EoL solar PV panels and reusing them to make new solar panels the actual number of waste (i.e., not recycled panels) could be considerably reduced. Scenarios involving recycling were analysed by Cucchiella and Rosa (2015) [64] based on net present value and discounted payback period rubrics with the aim of supporting management strategies in respect of recycling plants, with particular reference to the economic viability of plants of various sizes. A 2.6 MW conventional power station causes an annual volume of 1480–2220 t CO<sub>2</sub> eq emissions and this could be saved by recycling 186-ton solar PV waste. Such a saving would have a considerable positive impact on

the environment consequent upon the use of PV technology for electricity generation and would reduce emissions from power generation by around 49470 t CO<sub>2</sub> eq over the 20-life of a power station.

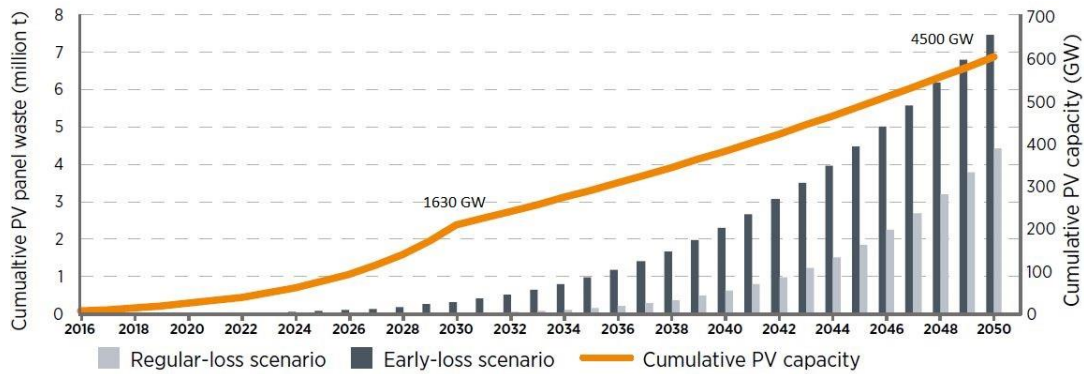


Figure 2. 7 The estimated cumulative worldwide solar PV module waste (tons) 2016-2050 [30, 31].

It has been estimated that the output from a 1903 MW conventional generating facility would be equivalent to recycling 1480 tons solar PV modules and would reduce emissions by around 11,840–17,760-ton CO<sub>2</sub> eq, over the lifetime of the plant, a saving equating to 396,770 t CO<sub>2</sub> eq. Moreover, Te recovery is important from both the environmental and economic perspectives. CdTe modules can be produced from recycled Te, thus cutting down the need to extract more of this limited natural resource.



## Chapter 3

### Materials and Methods

#### 3.1. Device simulation:

SCAPS-1D, version 3.3.0.1 was used to perform the simulation. The software was created by the University of Gent in Belgium. Any mathematical option which can explain the fundamental semiconductor calculations may be used for design Thin film solar cells (TFSCs). Poisson calculation [Eq. (1)], whole situation [Eq. (2)] and electron situation [Eq. (3)] were used, which are provided as follows:

$$\frac{d}{dx} \left( -\varepsilon(x) \frac{d\psi}{dx} \right) = q [p(x) - n(x) + N_d^+(x) - N_a^-(x) + p_t(x) - n_t(x)] \quad (1)$$

$$\frac{dp_n}{dt} = G_p - \frac{p_n - p_{no}}{\tau_n} - p_n \mu_p \frac{d\xi}{dx} \mu_p \xi \frac{dp_n}{dx} + D_p \frac{d^2 p_x}{dx^2} \quad (2)$$

$$\frac{dn_p}{dt} = G_n - \frac{n_p - n_{po}}{\tau_n} + n_p \mu_n \frac{d\xi}{dx^2} + \mu_n \xi \frac{dn_p}{dx} + \frac{D_n d^2 n_p}{dx^2} \quad (3)$$

where the permeability is  $\Sigma$ ; the electron charge is  $q$ ; generation rate is  $G$ ; diffusion coefficient is  $D$ ; electrostatic potential is  $w$ ; and the densities of the free electrons, free holes, trapped electrons and trapped holes are  $n$ ,  $p$ ,  $n_t$  and  $p_t$ , respectively. The ionised donor-like doping concentration and accepting doping concentration are  $N_d$  and  $N_a$ , respectively, whereas  $n$  is the electric field. In this analysis, perovskite planar structure Au/PEDOT:PSS/Perovskite/CdS/TCO/Glass was used in simulation. PEDOT: PSS was applied like an HTM for Au electrode for visible back contact, whereas the absorber layer was perovskite, and electron transport layer used CdS [24]. Common PEDOT:PSS was as an HTM for planar structure p-i-n hybrid perovskite-based solar cells [65]. The tuneable thickness of PEDOT:PSS material is 30 nm to 130 nm [65]. References state 50 nm as the optimum thickness, whereas the optimum bandgap is 2.2 eV, which is very low compared with bandgaps of other HTM layers. The conductivity of PEDOT:PSS varies from  $10^{-3} \text{ Scm}^{-1}$  to  $10^2 \text{ Scm}^{-1}$  [65]. Suitable

doping of PEDOT:PSS raises the number of holes and mobility of charges. Approximately 300 nm thickness of absorber layer of perovskite was considered in this simulation. The optimum absorber layer bandgap was measured as 1.5 eV, whereas 3.9 eV electron affinity for absorber layer was reported by other references. The comparative dielectric permeability ( $\epsilon_r$ ) is the ratio of the permeability of the material to the permeability of space. The role of  $\epsilon_r$  of perovskites has not been studied extensively, but it is widely used to detect the expected change on the functionality of conventional semiconductor [66]. A broad scale (from 6.5  $\epsilon_r$  to 60.9  $\epsilon_r$ ) [67,68] of dielectric permeability was observed for perovskite. Dielectric permeability is consistent for low frequencies, and the value is 60.9  $\epsilon_r$  within the range 20 Hz-1MHz [69]. The electron transport layer as a CdS was identified with a device constructed on additional transport materials; the CdS-based device presented a more complex  $V_{oc}$ , which is related to minor Fermi energy CdS and enhanced withdrawal.

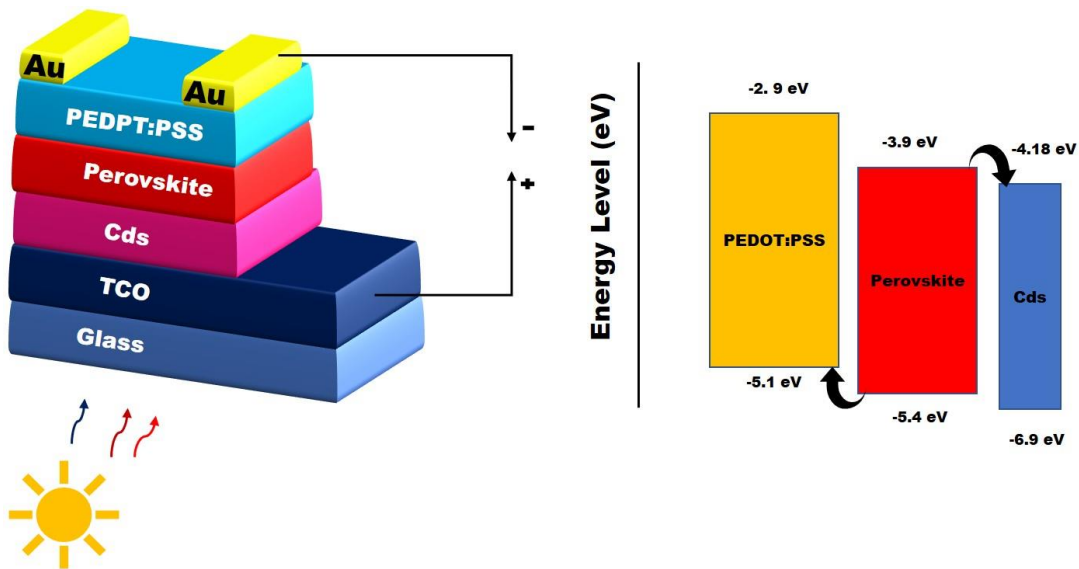


Figure 3. 1 Schematic perovskite tool construction and Energy level chart.

CdS is as a direct bandgap (2.4 eV) semiconductor with excellent electron transportability and is widely applied as an electron transport layer (ETL). Approximately 45 nm CdS thickness was applied based from references. In addition,  $350 \text{ cm}^2\text{V}^{-1}\text{s}^{-1}$  CdS layer electron mobility was applied to the simulation [24]. Different types of perimeter applied to the HTM, absorber and ETM, thereby affecting the J-V curve of the device. All optimum parameters are shown in this simulation.

Table 3. 1 List of parameters used in this mathematical simulation.

Parameter and unit	PEDOT: PSS	Interface	CH <sub>3</sub> NH <sub>3</sub> PbI <sub>3-x</sub> Cl <sub>x</sub>	CdS
Thickness (nm)	33		300-1000 variables	45
Bandgap (eV) E <sub>g</sub>	2.2 [69]		1.50 [70]	2.4 [71]
Electron Affinity (eV) λ	2.9 [69]		3.9 [14]	4.50 [72]
Dielectric Permeability (relative) ε <sub>r</sub>	3 [73]		10 [74]	10 [72]
Conduction Band Density (c/m <sup>3</sup> ) N <sub>c</sub>	2.2x10 <sup>15</sup> [73]		2.75x10 <sup>18</sup> [81]	2.2x10 <sup>18</sup> [72]
Valence Band Density (c/m <sup>3</sup> ) N <sub>v</sub>	1.8x10 <sup>18</sup> [73]		3.9x10 <sup>18</sup> [82]	1.9x10 <sup>19</sup> [72]
Electron Mobility (cm <sup>2</sup> V <sup>-1</sup> . S <sup>-1</sup> ) μ <sub>n</sub>	10 [73]		10 [84]	350 [14]
Hole Mobility (cm <sup>2</sup> V <sup>-1</sup> . S <sup>-1</sup> ) μ <sub>p</sub>	10 [73]		10 [84]	25 [76]
Acceptor Concentration N <sub>A</sub> (c/m <sup>3</sup> )	3.17 × 10 <sup>14</sup> [73]		1.0×10 <sup>9</sup> [14]	0
Donor Concentration N <sub>D</sub> (cm)	0		1.0×10 <sup>9</sup> [14]	1x10 <sup>18</sup> [14]
Radiative recombination coefficient (cm <sup>3</sup> s <sup>-1</sup> )	2.3x10 <sup>-9</sup>	3.0x10 <sup>-11</sup>	3.0x10 <sup>-11</sup>	2.3x10 <sup>-9</sup>
Cross Section for electrons and holes (cm <sup>2</sup> )		10 <sup>-19</sup>		
Gaussian defect energy Level (eV)				
Characteristics Energy (eV)				
Defect density N <sub>t</sub> (cm <sup>-3</sup> )	1 × 10 <sup>14</sup>	10 <sup>10-16</sup> variable	10 <sup>11-17</sup> variable	1 × 10 <sup>14</sup>

### 3.2. Solar cell preparation

The FTO glass substrate with the dimension of 3x3 cm<sup>2</sup> was given by Sigma-Aldrich, USA. The FTO thickness was 500 nm and had a normal sheet opposition around 16 Ω/sq. FTO was structured by carving with zinc powder and 3 M HCl. They were cleaned with a 2% Hellmanex solution and washed with de-ionized water, ethanol, (CH<sub>3</sub>)<sub>2</sub>CO(acetone), methanol, and dishwasher. Before applying the blocking layer, the glass substrate was cleaned using MAMDW rules (methanol for 10 min, (CH<sub>3</sub>)<sub>2</sub>CO(acetone) for 10 min, methanol for 10 min, and deionized water for 20 min) ultrasonic shower. The thick TiO<sub>2</sub> layer was set up by sputtering 60 min for 100 nm thickness (room temperature). In the wake of sputtering through to thermal strengthening chamber 3000 for 10 min. Upon cooling, the substrate was transferred to a nitrogen-filled Glove-box. A solution comprising PbI<sub>2</sub> (460 mg) by turn coating at 5000 rpm for 30 s and then heat treated at 100 °C for 30 min. Furthermore,

methylammonium iodide (160 mg) in 2-propanol was turned covered powerfully (at 5000 rpm, all out 50 s) onto the substrate. After 5 s, 100  $\mu\text{L}$  of chlorobenzene was included on top of the turning substrate, and then the substrate was set on a hot plate (100  $^{\circ}\text{C}$  for 30 min). The HTMs were then saved by turn coating at 2000 rpm for 40 s. The HTM was prepared by dissolving 80 mg of spiro-MeOTAD and 29 mL of 4-tert-butylpyridine, 18.5 mL of a conventional solution of 500 mg  $\text{mL}^{-1}$  lithium bis(trifluoromethylsulfonyl)imide in acetonitrile in 1.5 mL of chlorobenzene. The devices were stored medium-term under air at room temperature and <30% humidity to consider the oxidation of spiro-OMeTAD. The top anode was stored by thermal evaporation of gold (gold boiling point at 2600  $^{\circ}\text{C}$ ) under vacuum (at  $\sim 10^{-6}$  mbar) with a thickness of 40 nm (liquid nitrogen gas utilized for thermal evaporation).

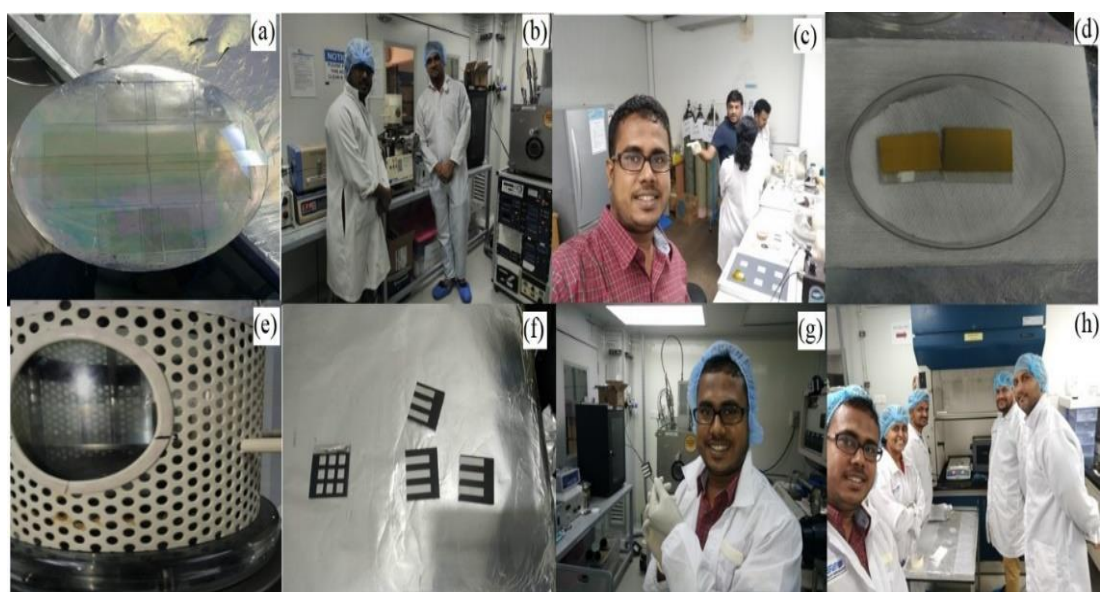


Figure 3. 2 Perovskite solar cell preparation: a) glass substrate ready for  $\text{TiO}_2$  deposition. b) With my supervisor during the deposition time. c) our research group Spin coating deposition. d) after  $\text{PbI}_2$  deposition. e) deposition electrode. f) during the annealing solar cell on hotplate. g) Finally made full cell. h) Me and my research group.

### 3.3.Solar cell recycling methodology:

#### 3.3.1. Layer by layer:

In this part, preferred P-PSCs for recycling, which was gathered from NARA Institute of Science and Technology. In the initial step, gold can be expelled by dissolving the opening transporter as depicted underneath, which caused delamination

of the gold anodes (Alternatively, gold can be removed using sticky tape). Gold can be gathered by a method for sanitization. The Spiro-OMeTAD layer was ejected by dunking the whole substrate in chlorobenzene while slowly turning the planning. After 3 min, the substrate was expelled from the solution and then dried under a nitrogen stream gradually. Different from chlorobenzene, ethyl acidic can be used to clear the opening transporter layer without causing corrosion.

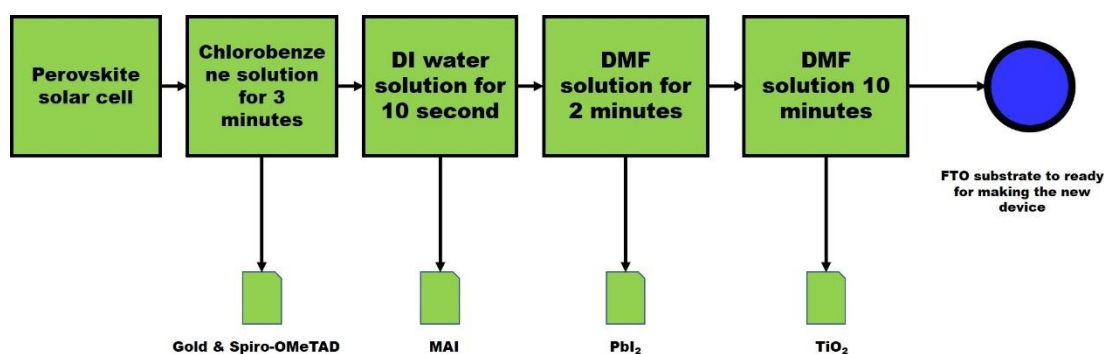


Figure 3. 3 Layer by layer recycle process of the planar structure of perovskite solar cell.

The Spiro-OMeTAD isolated from the chlorobenzene solution by utilizing revolving evaporator under vacuum. The chlorobenzene breaking point was  $132\text{ }^{\circ}\text{C}$ , and the Spiro-OMeTAD breaking point was  $>360\text{ }^{\circ}\text{C}$ . To expel the methylammonium iodide from the perovskite, the substrate was immersed in deionized water for around 10s and then dried under a nitrogen stream.

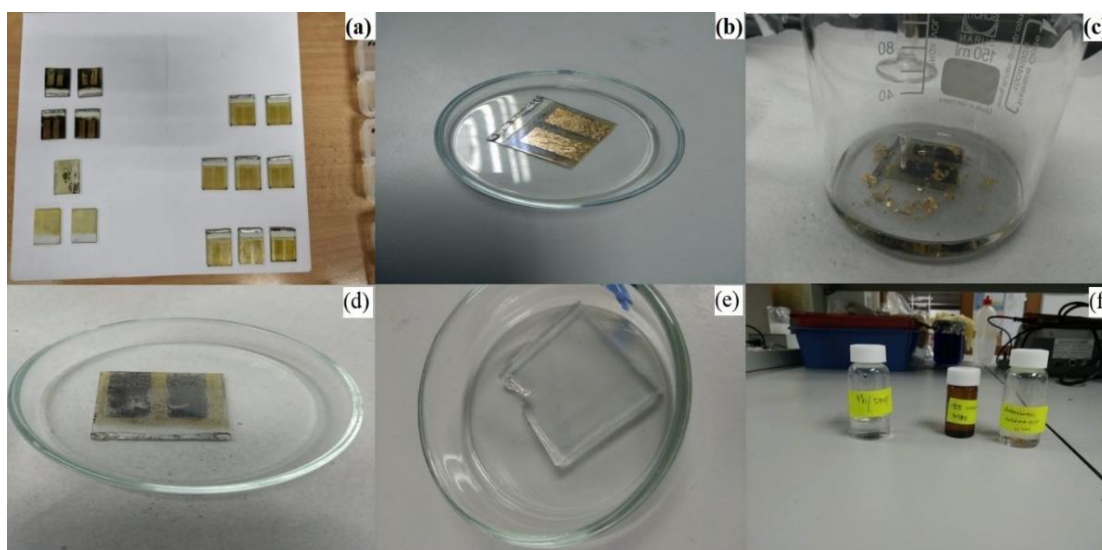


Figure 3. 4 (a) Perovskite solar cell for prepared recycle. (b) Selected the best cell for recycle. (c) removal of the gold and Spiro-OMeTAD layer. (d) After remove the cell

electrode and HTM layer prepare for absorber layer recycle. (e) After recycled the FTO coated glass substrate (f) Storage the liquid solution.

To eliminate the remaining water, the substrate was placed on a hot plate at 120 °C for 15 min. The accomplished PbI<sub>2</sub> layer was drenched for 2 min in DMF to break down PbI<sub>2</sub>. PbI<sub>2</sub> was estimated by UV-vis spectroscopy and ICP-MS examination. This solution can be used for recycling by utilizing the vacuum procedure. The glass/FTO/TiO<sub>2</sub> substrate was placed in a new DMF solution for 10 min to expel the TiO<sub>2</sub> layer, after which the FTO substrate was dried at 120 °C. Upon cooling, the FTO/substrate and gold can be utilized for the planning of new devices.

### **3.3.2. One step solution:**

The antireflective layer and p-I-n intersection can be expelled with the water regia solution. In various scratching steps, these layers are evacuated continuously with a few mineral acids and corrosive blends. The carving plans must be adjusted to various cell advancements. Various blends, such as HNO<sub>3</sub> + 3HCl, have been used. Water regia solution is typically a yellow, rosy orange, fuming fluid and has a quickly evolving piece. The standard molar proportion between concentrated hydrochloric corrosive and concentrated nitric corrosive (HCl:HNO<sub>3</sub>) was 3:1. Concentrated HCl is about 35%, and concentrated HNO<sub>3</sub> is about 65%; thus, the volume proportion is generally 4 sections concentrated hydrochloric corrosive to 1 section concentrated nitric corrosive. As indicated by the procedure, we prepared a 12 mL lab-scale water regia solution containing 9 mL of HCL corrosive and 3 mL of HNO<sub>3</sub>.

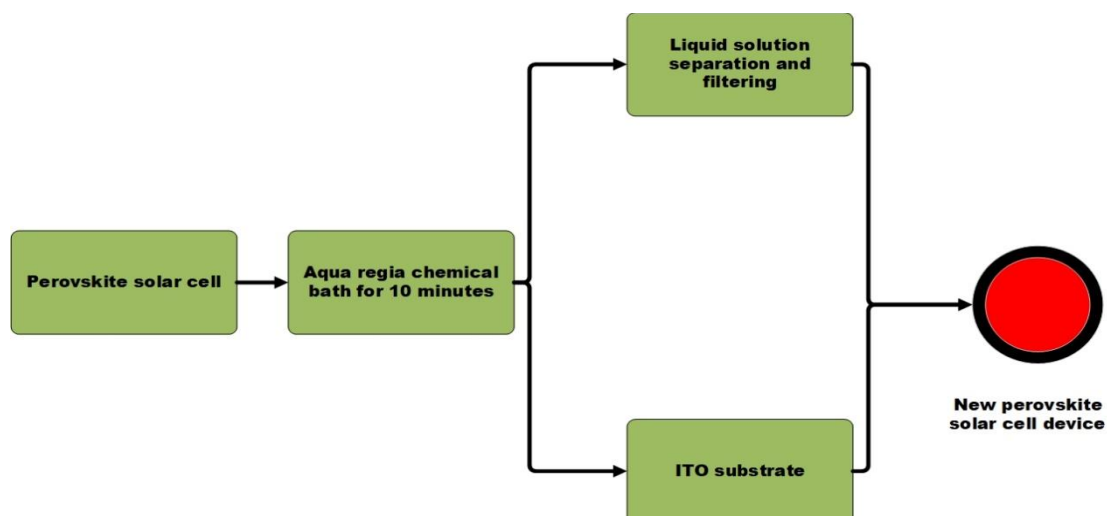


Figure 3. 5 One step aqua regia chemical bath process.

In this procedure, in order to expel the gold, HTM, absorber layer, and ETL with one solution and recouped the ITO/substrate effectively.

After this procedure, the substrate was expelled from the solution and then dried under a nitrogen stream gradually, after which the ITO substrate was dried at 120 °C on a hot plate. Upon cooling, the ITO substrate can be used for another device.

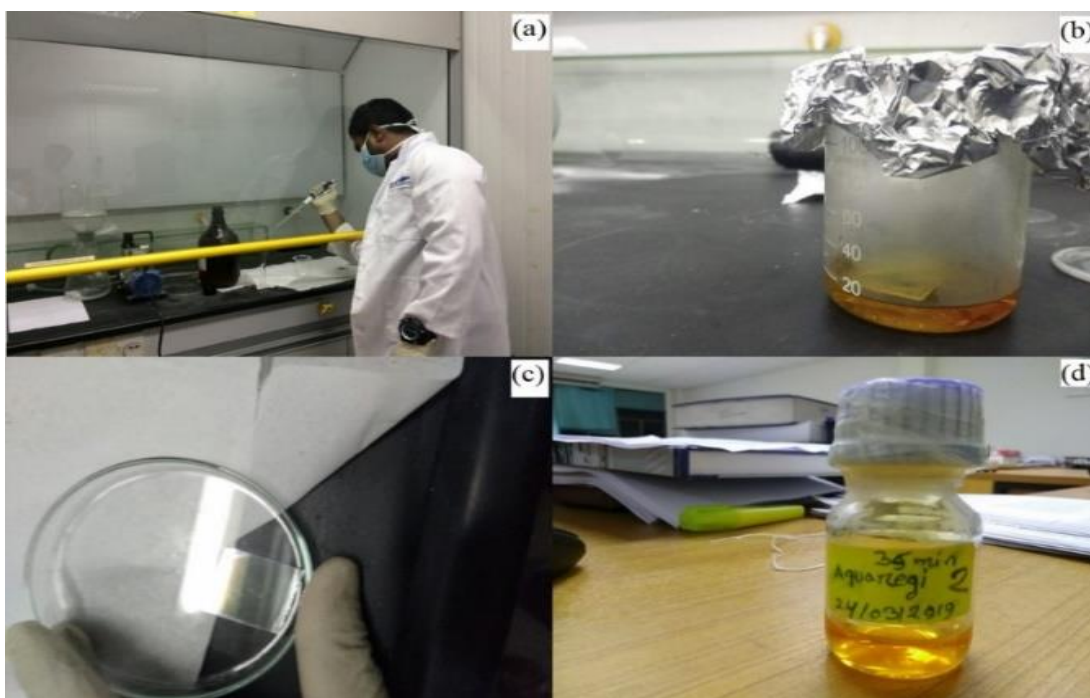


Figure 3. 6 One step recycle process: a) Prepared aqua regia solution. b) solar cell chemical bath into the jar recovered ITO glass substrate. d) storage used chemical for analysis.

### 3.4. Device characterization:

Scanning electron micrographs were obtained on a ZEISS SURRA 55VP magnifying lens. The cross-areas were sectioned directly before the estimation. The essential structure was examined by energy dispersive X-ray (EDX) with an EDX locator from OXFORD INSTRUMENTS. X-ray diffraction patterns of the gold powder were acquired on an STOE powder diffractometer in a transmission geometry (Cu  $K\alpha_1$ ,  $\lambda = 1.5406 \text{ \AA}$ ) outfitted with a Mythen-1K indicator. X-ray diffraction analysis of the perovskite films was conducted in reflection mode utilizing a Bruker D8 Discover with Ni-sifted Cu  $K\alpha_1$ -radiation ( $\lambda = 1.5406 \text{ \AA}$ ) and a position-touchy semiconductor locator (LynxEye). Proton atomic attractive resonance (H-NMR) was taken at 399.65 MHz with a JNM-GSX270 Fourier-Transform Spectrometer. DMSO-d6 (Spiro-omeTED was broken up) was utilized as the dissolvable with a centralization of 20% w/v. Each single chemical move was accounted for in parts per million (ppm). Consistent-state UV-Vis assimilation spectra were procured with a Lambda 1100 UV-Vis spectrophotometer. Inductively coupled plasma mass spectrometry Elan (ICP-MS-9000) estimation was completed by utilizing Perkin Elmer Sciex. Hall impact estimation was utilized recognizing the resistivity, bearer fixation, versatility, and conductivity by the Ecopia corridor impact estimation system (HMS-3000 VER 3.5.5). J-V twists were recorded with a Keithley 2400 source meter under numerical AM 1.5G solar light, with an event force of about  $100 \text{ mWcm}^{-2}$ , which was reviewed for the positive light power using a Fraunhofer ISE silicon cell. The qualities of the devices were assessed from the determined J-V bends accomplished from the rearward check (from  $V_{oc}$  to  $J_{sc}$ ). Each device showed a considerable amount of hysteresis concerning the ahead and in invert check, which is tantamount for every test. The dynamic territory of the solar cells was characterized by a square metal gap veil of  $0.0831 \text{ cm}^2$ .



## Chapter 4

### Result and Discussion

#### 4.1. Simulation result:

##### 4.1.1. Effect of absorber layer defect on different thickness:

The band diagram of the p-i-n HVPSCs in equilibrium condition is shown in Figure 3.1. An energy barrier of 0.6 eV is present between the conduction band minimum ( $E_c$ ) and the lowest unoccupied molecular orbital (LUMO) of the absorber layer, which are between height occupied molecular orbitals (HUMO) of both absorber layers. Transition levels characterised either as Fermi level position located near the CBM (VBM) or within the forbidden band of absorber layer are formed [23]. The electrical output parameter extracted of inserted solar cell indicated a low radioactive recombination and long diffusion length of charge carrier due to the low excitation of bounding energy [77]. The absorber layer of perovskite solar cell needed to absorb the maximum number of photons energy (electron-hole pair) works in two ways, as follows: (1) fewer electrons participate in the generation process; and (2) leads to the reduced fill factor and efficiency. The absorber layer thickness should be optimum. The thickness of the perovskite layer varies from 300 to 1000 nm. According to the simulation, when thickness is rapidly decreased, the material bandgap chooses the extreme probable  $V_{oc}$  of that material, such that  $V = -E_g / q$ , where the band gap energy is  $E_g$  at 0 K temperature [12, 32]. However, the determined value of  $V_{oc}$  is less than the threshold set by the bandgap energy, as follows:

$$V_{oc} = \frac{KT}{q} \ln \left( \frac{J_{sc}}{J_0} + 1 \right) \quad (1)$$

where the light-generated current is  $J_{sc}$ , and the recombination current is  $J_0$ . The thermal voltage is  $KT/q$ , in which the Boltzmann constant is  $K$ , and the temperature is  $T$ . Thus, Eq. (1) states that lower  $J_0$  increases  $V_{oc}$ . Superior defect density triggers elevated recombination proportion in the average perovskite solar cell that decreases the dispersal length of charge carriers, which is beneficial for the lifetime of

carriers. Correa-baena et al. examined carrier density and open-circuit voltage controlled by the bulk charge density [21]. The generated charge carrier in absorber layer can recombine via both bimolecular and trap-assisted mechanism. The biomolecular recombination rate (RBR) is given as follows:

$$R_{BR} = k_{BR}(np - n_i^2) \quad (2)$$

where the biomolecular recombination constant is  $K_{BR}$ , and the intrinsic carrier density is  $n_i$ . Shockley-Read-Hall (SRH) recombination may clarify the conceivable recombination components to decide the impact of deformity thickness on the use of hybrid perovskite solar cell, which is shown as follows:

$$R_{SRH} = \frac{C_n C_p \Sigma_T}{C_n(n + n_1) + C_p(p + p_1)} (np - n_i^2) \quad (3)$$

where the capture coefficients for electrons and holes are  $C_n$  and  $C_p$ , respectively.  $C_n$  denotes the probability per unit time that the electron in the conduction band takes in case the defect is filled with a hole and is able to capture the electron. Jongseob et al. reported the formation of the shallow level to trap electrons affected by Br incorporation and deep level trap through the interaction of dangling Pbs [20]. The solar cell generates the maximum voltage, whereas the open-circuit voltage reflects the maximum energy that can be separated from any consumed photon and the distinction in terms of the capability of the most minimal vitality ingested by the photon. Moreover, the generated charge and the open-circuit potential under full sunlight can be considered as simple measurements of the fundamental energy loss or “loss-in-potential” in a solar cell [78]. Figure 4.1 and 4.2 show curve displays of perovskite working factors affecting defect density and layer thickness variables, respectively. The effect of defect density from  $10^{11}$  to  $10^{17}$   $\text{cm}^{-3}$  and thickness from 300 to 1000 nm are analysed to assess the device performance. Additionally, a situation vitality level of 0.6 eV is established based on the conduction band and with Fermi level mid-point as the position. All other parameters are kept unchanged to investigate the gadget execution. Device performance

strongly depends on absorber layer thickness. As shown in the graph (Figure 4.1),  $V_{oc}$  depends on the variability of both absorber layer thickness and defect density level. The defect with low structure energy creates shallow-level defect, which results in long electron-hole diffusion length and high  $V_{oc}$  [75]. In addition, a trap with deep levels obtain high composition vitality that results in an unpleasant impact on the electron to hole dispersion length and open-circuit voltage [15]. The highest and lowest  $V_{oc}$  levels were observed to be 1.21 and 0.86 V, respectively, when absorber layer thickness is 300–400 nm, and defect level is  $10^{11}$ – $10^{11}$ . Figure 4.1 shows a defect level of  $10^{11}$ – $10^{15}$ , which indicates a low defect (small change) of open-circuit voltage. When defect level decreases from  $10^{16}$  to  $10^{17}$ , deep defect occurs. When the absorber layer thickness increases, the open-circuit voltage slowly decreases. As the thickness expanded to 500–700 nm,  $V_{oc}$  is almost constant (defect density,  $10^{11}$ – $10^{14}$   $\text{cm}^{-3}$ ). When the defect density reaches  $10^{15}$ – $10^{17}$   $\text{cm}^{-3}$ , the open-circuit voltage level significantly faults on simulation (Figure 4.1), which can be due to the enhanced recombination of carriers in the deeper absorber. The increase in thickness from 800 nm to 1000 nm results in a  $V_{oc}$  of 1.8 V at a defect density of  $10^{11}$ – $10^{13}$   $\text{cm}^{-3}$ ; variation of absorber layer thickness and defect density significantly change the  $V_{oc}$ . When defect density increases to  $10^{14}$ – $10^{17}$   $\text{cm}^{-3}$ , the  $V_{oc}$  rapidly changed. Lui reported that increase in absorber layer thickness results in shunt resistance drop. The increased electron current contribution to the forward diode subsequently reduces the  $V_{oc}$ . The  $J_{sc}$  shows very insignificant variation for the different combinations of defect density and the thickness of the absorber layer. The simulation result is shown in Figure 4.1 (b), where  $J_{sc}$  is shown to increase sharply from 21.85  $\text{mA}/\text{cm}^2$  to 26.94  $\text{mA}/\text{cm}^2$ , whereas perovskite absorber layer thickness improved from 300 nm to 1000 nm, as a result of  $10^{11}$   $\text{cm}^{-3}$  defect density. When changed the defect density and thickness, small changes on  $J_{sc}$  are observed, until it reaches  $10^{15}$   $\text{cm}^{-3}$ . In comparison, when increase the defect density to  $10^{16}$ – $10^{17}$   $\text{cm}^{-3}$ ,  $J_{sc}$  consequently changed. In another situation, when defect density reaches  $10^{17}$ , the absorber layer thickness rapidly increases, but  $J_{sc}$  dramatically decreases. Despite only being a function of open-circuit voltage, the fill factor does not only depend on the open-circuit voltage similar with recombination processes in the weakening area [78]. Expanding the thickness avoids such contact, bringing about enhancements to both FF and  $V_{oc}$ . These are all predictable with the minimal fill factor and give a clarification of

the unfortunate changes in  $V_{oc}$ . When the perovskite thickness is enhanced, the recombination resistance raises consequently, which is related to the associated rise in FF and  $V_{oc}$ . The same connections have recently been seen between the recombination opposition and  $V_{oc}$  in planar heterojunction perovskite solar cells.

Conclusively,  $PCE = V_{oc} \times J_{sc} \times FF$  equation suggests that the efficiency is a merger of the three output parameters reflected overhead and based on the consequence of open-circuit voltage and fill factor variation in this study. Efficiency is recorded as 20% to 25% when increase the thickness from 300 to 1000 nm, and defect density is at  $10^{11} \text{ cm}^{-3}$ . Makhsud et al. experimentally showed a higher defect density up to  $10^{16}$ – $10^{17} \text{ cm}^{-3}$  [15]. Temporarily, the absorber thickness is not exactly the dispersion length of carrier. A large portion of the photogenerated carrier can achieve the relating terminal to create control, and hence, the efficiency increments. The efficiency significantly diminished from 25% to 10% as the trap density increases from  $10^{11}$  to  $10^{17} \text{ cm}^{-3}$ , and thickness increases from 300 nm to 1000 nm.

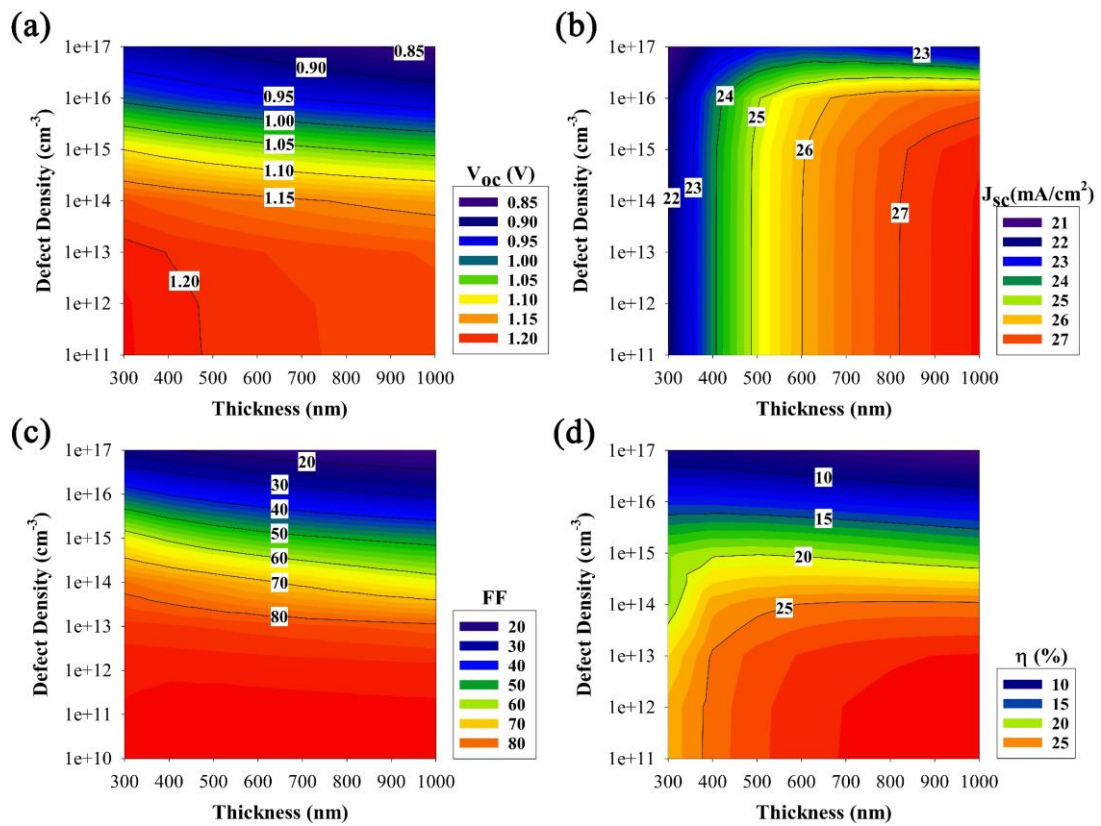


Figure 4. 1 Outline displays of perovskite solar cell show limitations colony on absorber defect density and thickness.

#### 4.1.2. Effect of defect on ETL interface CdS/perovskite absorber layer with thickness:

The interface layer value is significant for solar cell consummation. To discover the impact of the interface quality on sunlight-based cell execution, to change the trap concentration and absorber layer of the CdS/absorber interface from  $10^{10} \text{ cm}^{-3}$  to  $10^{16} \text{ cm}^{-3}$ . In addition, change the absorber layer and keep the other parameters at the default values. Huge series resistance (Rs) linked to the CdS/absorber interface contact is regarded as the major consequence of low efficiency of CdS film-based hybrid perovskite solar cell [79]. This is attributed to the diffusion of metal cations into the halide perovskite (HaP) during crystallisation on the inorganic HTLs. The occurrence of perovskite solar cells can be adjusted by defects. Structural defects of two unique materials prompts principal interfacial deformities, which cause charge recombination in the PSCs. Figure 4.2 shows the impact of interfacial trap thickness of CdS/Perovskite layer on the device execution. As show, the interface value of CdS/absorber layer considerably affects solar cell execution [80]. The effects of defects on the p-i-n PSC performance are obtained by considering the two main types of interfacial defects: substitution defects and oxygen vacancy ( $V_o$ ). Defect density ( $10^{10} - 10^{16} \text{ cm}^{-3}$ ) and the thickness of the absorber layer (300 nm to 1000 nm) are examined. The perovskites below the lowest conduction band is selected at 0.6 eV in the process of the mention (put into the simulation software). Figure 4.2 (a) demonstrates the reliance of  $V_{oc}$  on the trap density and thickness of absorber layer. The highest  $V_{oc}$  recorded is 1.20 V, and the lowest is 0.95 V. According to the result, when increase the thickness to 300–500 nm and defect density to  $10^{10} - 10^{11} \text{ cm}^{-3}$ , an almost equal  $V_{oc}$  of around 1.2 V is obtained. When the hand thickness increases rapidly, the  $V_{oc}$  slowly decreases, whereas the defect density remains same. In addition, when increasing the defect density significantly to  $10^{12} - 10^{16} \text{ cm}^{-3}$ , the  $V_{oc}$  rapidly decreases. When the defect density reaches  $10^{15} \text{ cm}^{-3}$ , the interface layer has a deep trap (located at low  $V_{oc}$ ). When increase the absorber layer thickness (500–1000 nm) rapidly, the  $V_{oc}$  decreases slowly, defect density is  $10^{11} \text{ cm}^{-3}$ . When defect density increases, the resulting  $V_{oc}$  increases, as described before. The thickness of states (TOS) of both devices are further evaluated

from the angular frequency, dependent on capacitance measurements with the following equation:

$$TOS = \frac{N_{t,0}}{k_B T_0} \exp\left(\frac{E_F - E_C}{k_B T_0}\right) \quad (4)$$

where the total density of the localised state is  $N_{t,0}$ , and the unit of temperature is  $T_0$ , which replicates the size of the defect spreading meaning underneath the superiority of conduction band energy level ( $E_c$ ). A higher value of  $T_0$  implies a broader TOS [80,81]. The deviation of t-TOS dissemination was detected by obtaining the capacitance through electronic impedance spectroscopy at open circuit.

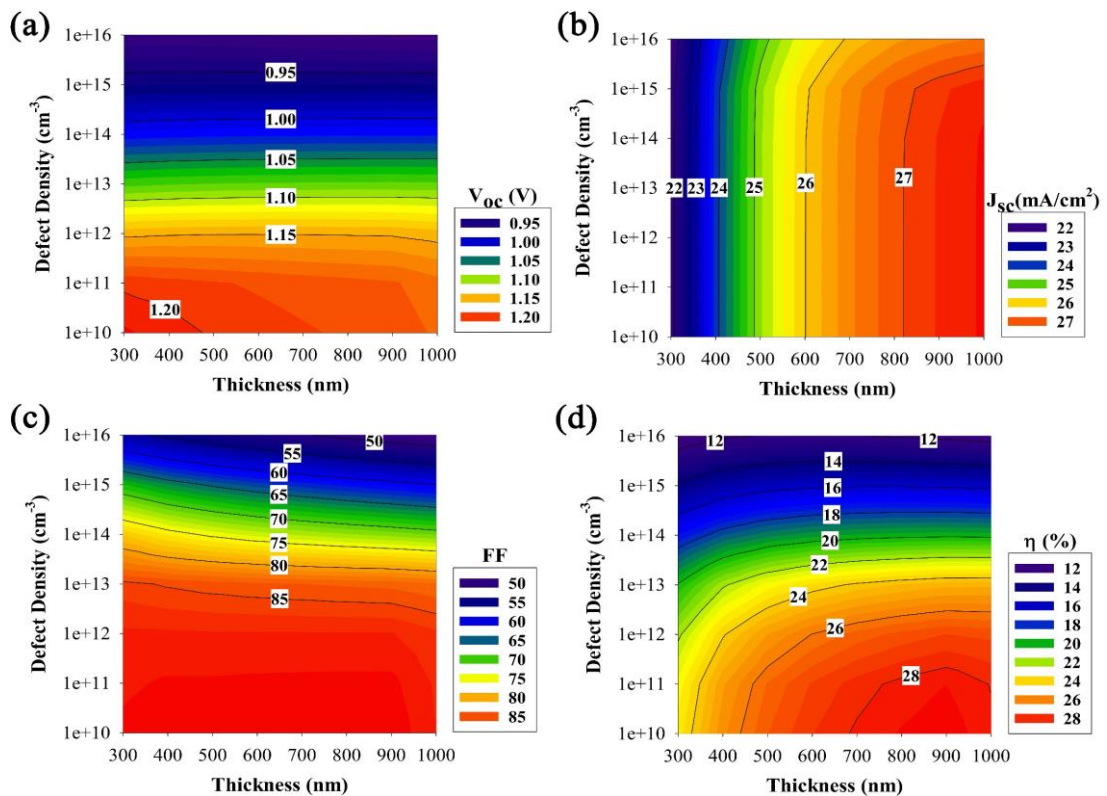


Figure 4. 2 Outline displays of perovskite solar cell show limitations colony on defect density of CdS/perovskite interface and perovskite's thickness.

The capacitance in this type of dimension is comparable to t-TOS. Capacitance reproduces the capability of a photovoltaic device to accept or release supplementary charge carriers as an outcome of changes in quasi-Fermi level. As shown in Figure 4.2 (b),  $J_{sc}$  increases when increase the absorber layer thickness. The highest  $J_{sc}$  is 27 mA/cm<sup>2</sup> when the absorber layer thickness reaches 1000 nm, whereas the lowest  $J_{sc}$  is 22 mA/cm<sup>2</sup> when the absorber thickness is 300 nm. An increase in the

absorber layer thickness causes the increase in defect density.  $J_{sc}$  value slowly decreases when defect density increases to  $10^{14}$ – $10^{16}$   $\text{cm}^{-3}$ . Trap thickness has no impact on the FF beyond this scale. The FF significantly shifts and doubles when the defect thickness changes from  $10^{13}$  to  $10^{16}$   $\text{cm}^{-3}$ . Figure 4.2 (c) shows that trap density of ETL/absorber interface layer has a significant effect on the PCE of PSCs, whereas Figure 4.2 (d) shows that the trap thickness of ETL/absorber interface layer affects the efficiency of PSCs. The efficiency increases from 22% to 28% as perovskite absorber thickness increases from 300 nm to 1000 nm as a result of defect density. Moreover, small changes in cell efficiency occur when defect density is  $10^{10}$ – $10^{13}$   $\text{cm}^{-3}$ , whereas a significant decrease occurs when defect density reaches  $10^{14}$ – $10^{15}$   $\text{cm}^{-3}$ . When defect density reaches  $10^{16}$   $\text{cm}^{-3}$ , recombination is high; an increase in charge recombination is observed as absorber layer thickness increases [83,84,85]. The increase of thickness from 300 nm to 1000 nm raises the efficiency from 11.21% to 11.51%.

#### **4.2. Performance of perovskite solar cell:**

The PV characteristics of the reference planar perovskite device were analysed, and the J-V characteristics are depicted in Figure 4.3. The typical deviations of photovoltaic factors such as PCE,  $V_{oc}$ ,  $J_{sc}$ , and FF were 4.7%, 0.71 V, 12.79  $\text{mA cm}^{-2}$  and 0.5%, respectively.

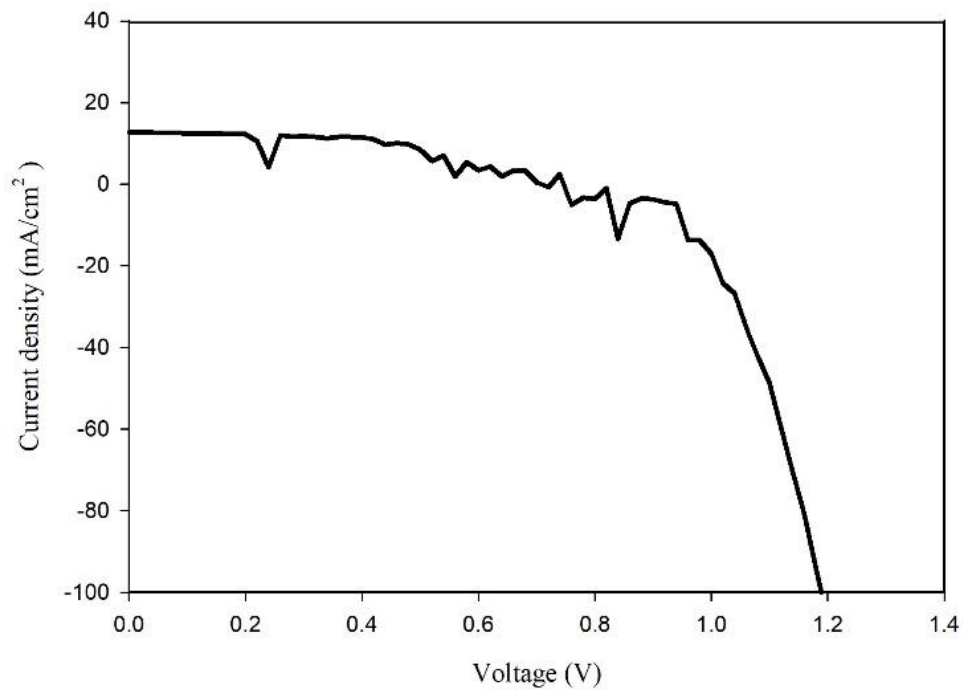


Figure 4. 3 JV characteristics of the planar structure perovskite solar cell.

#### 4.3. Recycle characters layer by layer:

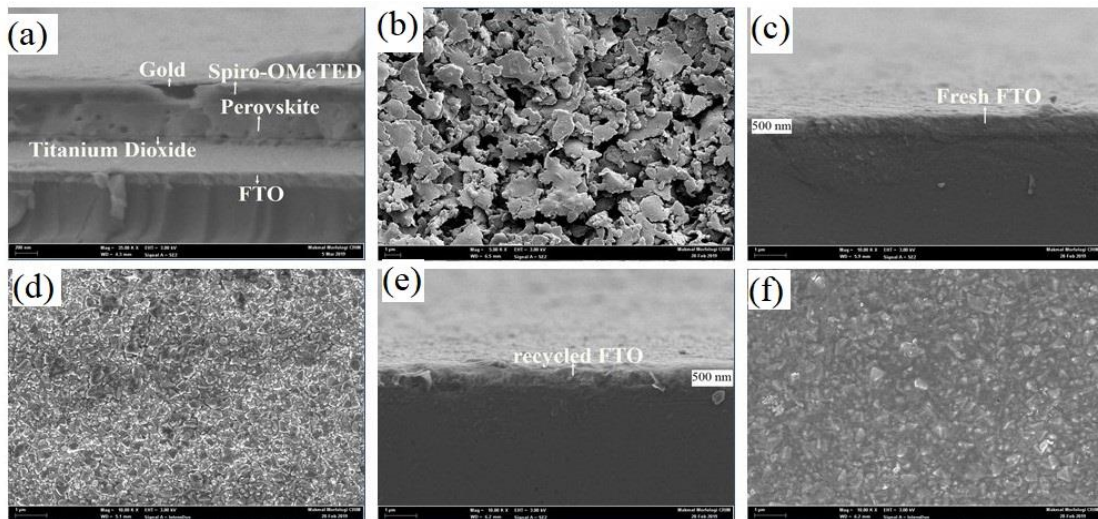


Figure 4. 4 a) SEM micrograph cross-sectional of the full cell device. b) Top view of the full cell. c) Cross-section of the fresh FTO coated glass. d) Top view of fresh FTO coated glass. e) cross-section of recycled FTO coated glass. f) Top view of recycled FTO coated glass.

Figure 4.4 shows the top-view and cross-sectional scanning electron micrographs of the full cell and before recycling (c) and after recycling (e) treatments



of the FTO-coated glass substrate. Cross-sectional view of the FTO-coated glass shows that no materials remained on the surface after the treatments. Figure 4.4 (e+f) shows that the absorber layer, HTM and electrode layer treatments did not affect the FTO substrate. No detrimental effects of the dismantling process, such as delamination or scratching of the photoanode, were observed. The FTO layer remained completely intact.

#### 4.3.1. Trace Pb and Spiro-OMeTAD by UV-vis spectroscopy:

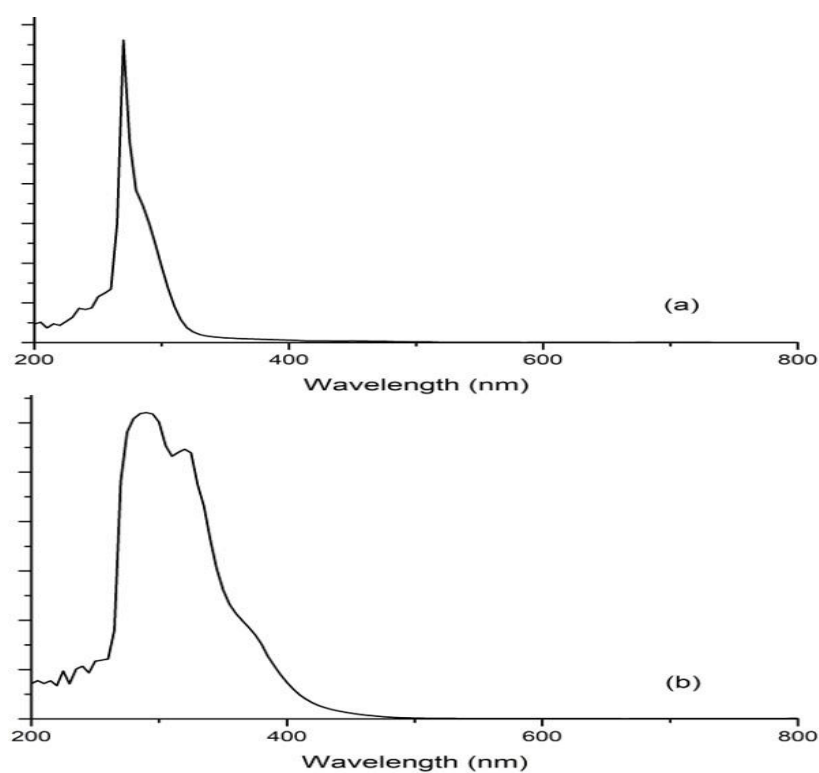


Figure 4. 5 UV-Vis absorption spectra of (a) DMF containing extracted lead iodide and (b) reference solution of commercial lead iodide dissolved in DMF.

The solvents used for solar cell recycling were studied using UV-vis, and the results are presented in Figure. The area of the solar cell for recycling was  $3 \times 3$   $\text{cm}^2$ .

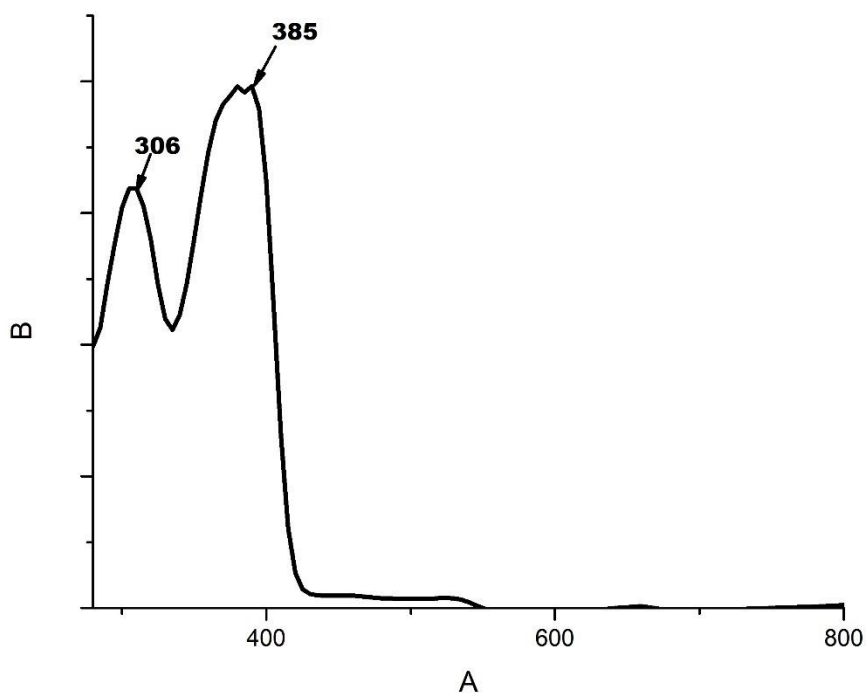


Figure 4. 6 Chlorobenzene including obtained Spiro-OMeTAD.

A 12 mL solution of chlorobenzene was used to remove Spiro-OMeTAD and gold, 12 mL of DI water to remove MAI and 12 mL of DMF to remove  $\text{PbI}_2$ .

The chlorobenzene solution clearly showed the absorption of Spiro-OMeTAD in UV-vis and its oxidised species, which gives a signal in the range of 300–400 nm. Lee et al. described that the Spiro-OMeTAD max range of absorbance peak is 306–385 nm [1]. Figure 4.6 shows that the absorbance wavelength peak ranges from 306 nm to 385 nm, which qualitatively ensures the presence of Spiro-OMeTAD.

The DMF solution containing  $\text{PbI}_2$  showed an absorption with an onset around 410 nm. No absorption was observed in the range of 450–550 nm, indicating the absence of other materials. We prepared a  $0.0025 \text{ mgmL}^{-1}$   $\text{PbI}_2$  solution in DMF with an absorption range of 300–410 nm as reference Figure 4.5 (b). The absorption of the DMF solution from the recycling is marked in the Figure 4.5 (a). It has examined

the lab-scale solar cell. However, the  $\text{PbI}_2$  and Spiro-OMeTAD from UV-vis analysis were probed qualitatively.

#### 4.3.2. Qualitative of Spiro-OMeTAD:

The recycled Spiro-OMeTAD was obtained by H-NMR ( $\text{DMSO-d}_6$ ). NMR spectroscopy is an analytical technique that aids in interpreting the molecular structure of a sample. The recycled Spiro-OMeTAD did not show any traces of the absorber layer material or methylammonium iodide. Figure 4.7 shows that the signal is 7 ppm, indicating the presence of functional group a of aromatics. According to the Spiro-OMeTAD result evaluation qualitatively proved. The arrangement of the carbon–hydrogen (Figure 4.8) framework within the structure can be further validated from the spectral peaks.

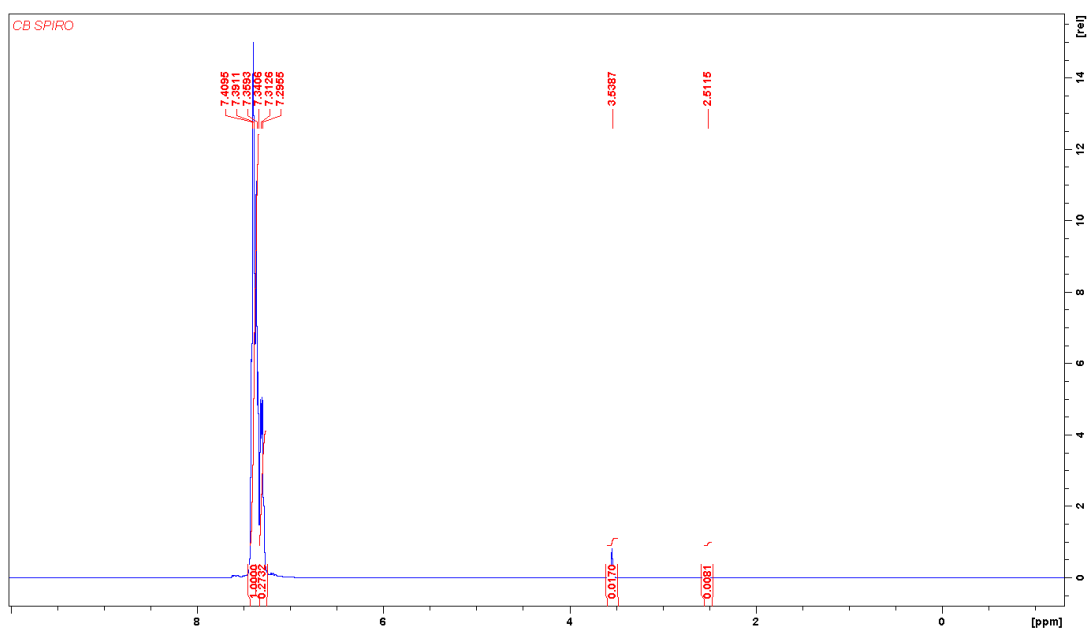


Figure 4. 7  $^1\text{H}$ -NMR spectroscopy of recycled Spiro-OMeTAD and  $\text{DMSO-d}_6$  pick.

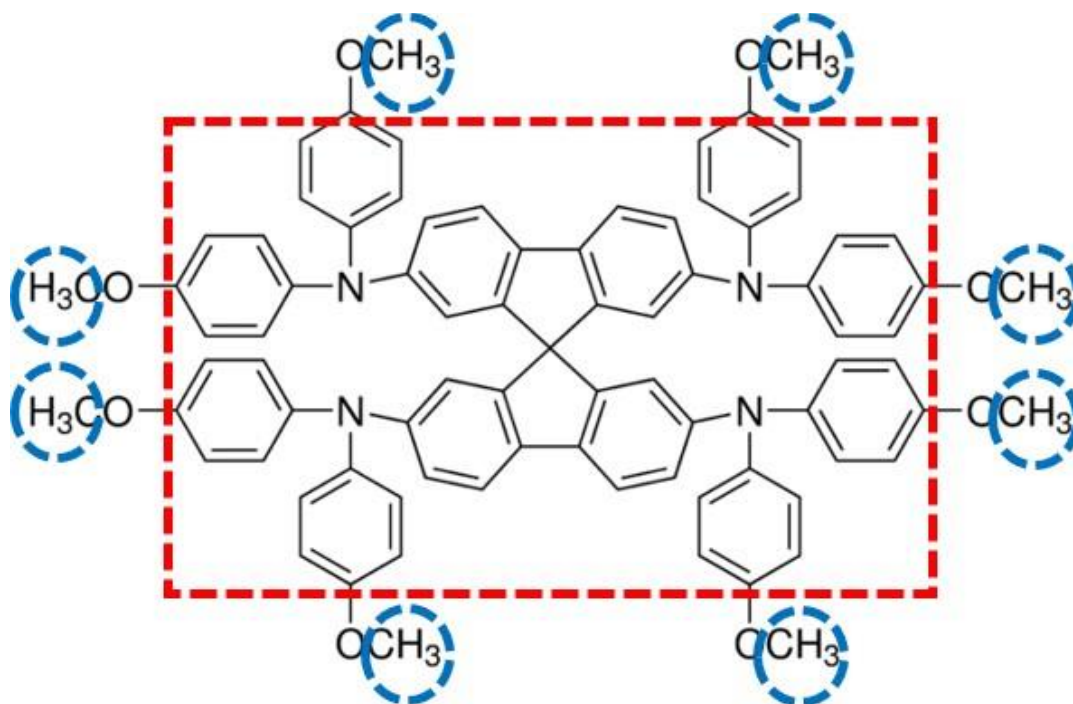


Figure 4. 8 H bond of Spiro-OMeTAD recycled powder.

#### 4.3.3. Quantitative analysis by ICP-MS measurement:

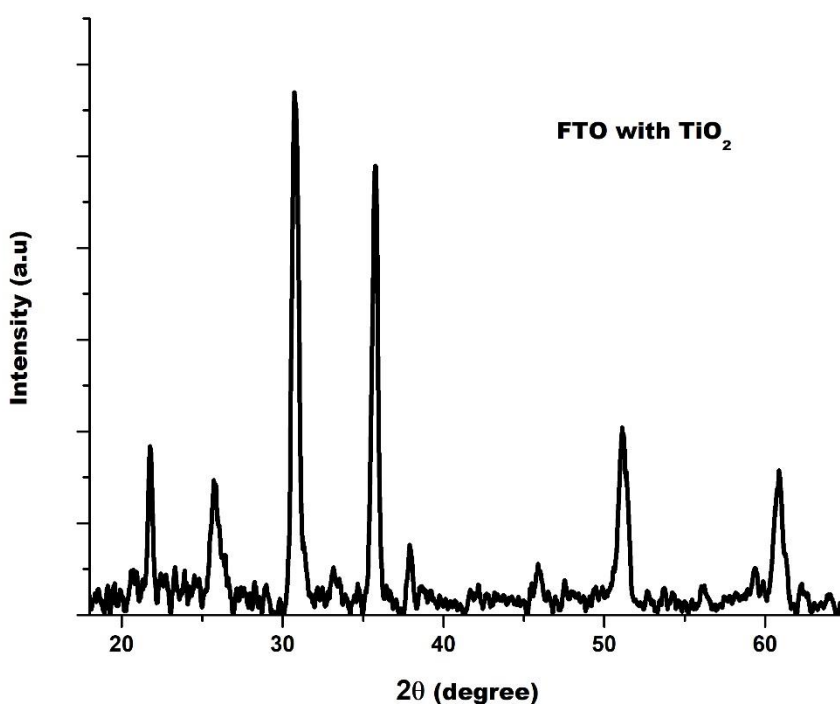
The solutions used in the ICP-MS measurements were the same as those in the UV-vis experiments. These solutions were measured with ICP to check for the presence of lead and titanium. The very low concentrations of lead in water can be ascribed to the short immersion time and relatively low solubility of  $\text{PbI}_2$  in water. The concentration of titanium in all samples was below the detection limit ( $0.0078 \mu\text{g mL}^{-1}$ ), indicating that the electron blocking layer did not dissolve during the recycling process and was simply delaminated. This result is expected because  $\text{TiO}_2$  is insoluble in these solvents. ICP measurement results showed that the DI water fraction used for the extraction of MAI contained  $17.72 \mu\text{g mL}^{-1}$  lead. Ascribe the very low concentrations of lead in the water to the short immersion time and relatively low solubility of  $\text{PbI}_2$  in water. Water containing at least  $5 \mu\text{g mL}^{-1}$  lead is considered hazardous according to the US Environmental Protection Agency (EPA, Federal Hazardous Waste code D008). The water fraction containing the recovered MAI is therefore below the maximum concentration of contaminants for toxicity characteristic according to EPA. The concentration of the DMF fraction, which was used for the extraction of lead iodide, was  $40.22 \mu\text{g mL}^{-1}$ . The result of ICP-MS quantitative recovery rate was obtained.

Table 4. 1 Metal concentrations measured by ICP-MS.

Solution	Pb( $\mu\text{g mL}^{-1}$ )	Ti ( $\mu\text{g mL}^{-1}$ )
DI Water	17.42	0.0078
DMF	40.22	0.322

#### 4.3.4. Qualitative and quantitative analysis for recycled FTO substrate:

Structural characterisation by X-ray diffraction was carried out on twin samples (Figure 4.9). XRD analysis was performed to verify the purity of each projected time after the subsequent flush treatment measurements.

Figure 4. 9  $\text{TiO}_2$  after the removing  $\text{PbI}_2$ .

The  $\text{TiO}_2$  blocking layer appeared after removing the  $\text{PbI}_2$  by immersing in DMF. Figure 4.9. clearly shows the presence of the  $\text{TiO}_2$  layer. This result is consistent with the XRD qualitative analysis of the FTO glass substrate after the treatment.

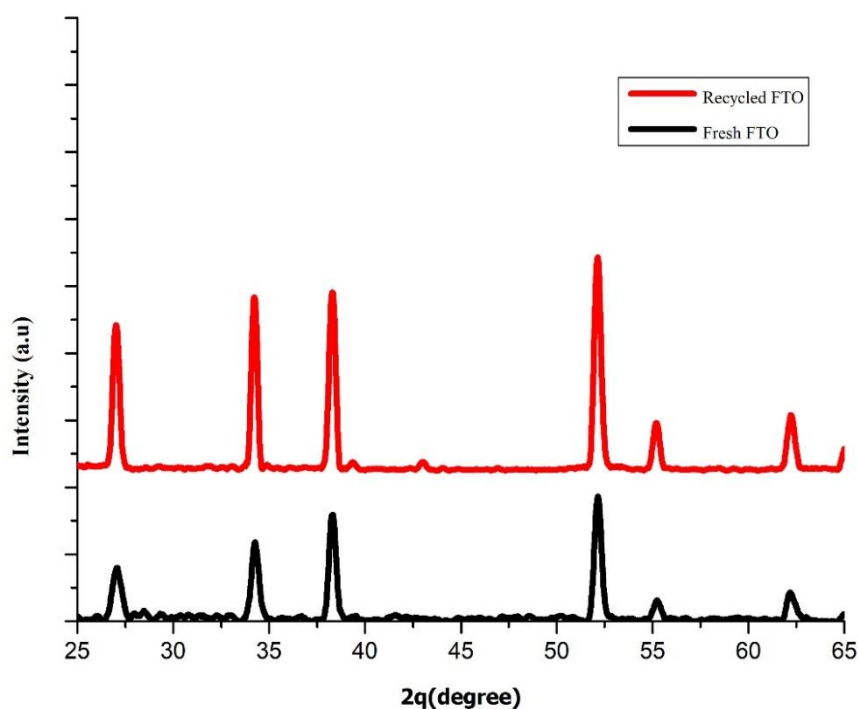


Figure 4. 10 X-ray diffraction (XRD) analysis: a) Fresh FTO glass substrate b) Recycled FTO glass substrate.

No titanium was observed on the recycled FTO substrate, indicating the complete removal of the blocking layer in Figure 4.10. XRD analysis showed that  $\text{TiO}_2$  was successfully removed on top of the FTO substrates. No significant differences were found between the fresh FTO and recycled FTO substrates. The thicknesses of the two samples were also similar. Figure 4.11. (a+b) shows the FTO glass substrate before and after the treatment. EDX analysis showed that the percentage of  $S_n$  was 72.9%, where recycled  $S_n$  was 70.8 % in the FTO glass substrate and other elements slightly unchanged. These results qualitatively and quantitatively proved that 99% of the FTO glass substrate can be recovered.

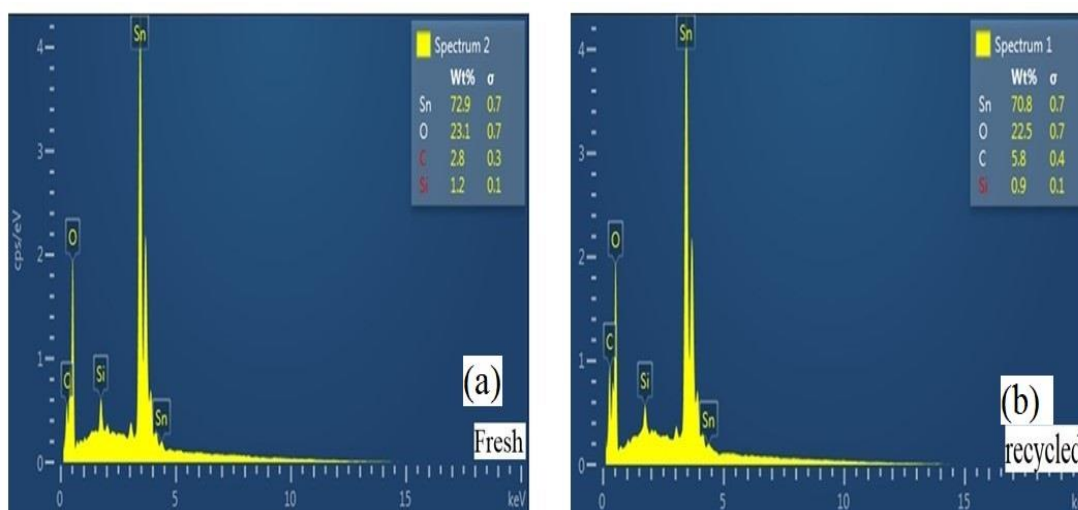


Figure 4. 11 Energy-dispersive X-ray spectroscopy (EDX), a) Element percentage of fresh FTO substrate b) element percentage of recycled FTO substrate.

The transmittance of the substrate was obtained by UV-vis absorption for fresh FTO and recycled FTO, and the results are given in Figure 4.12. The maximum transmittance was over 90%, where the absorption wavelength was around 500 nm. The standard transmittance of fresh and recycled FTO was across 85% for most of the visible spectrum. No significant differences were found between the fresh and recycled FTO substrates.

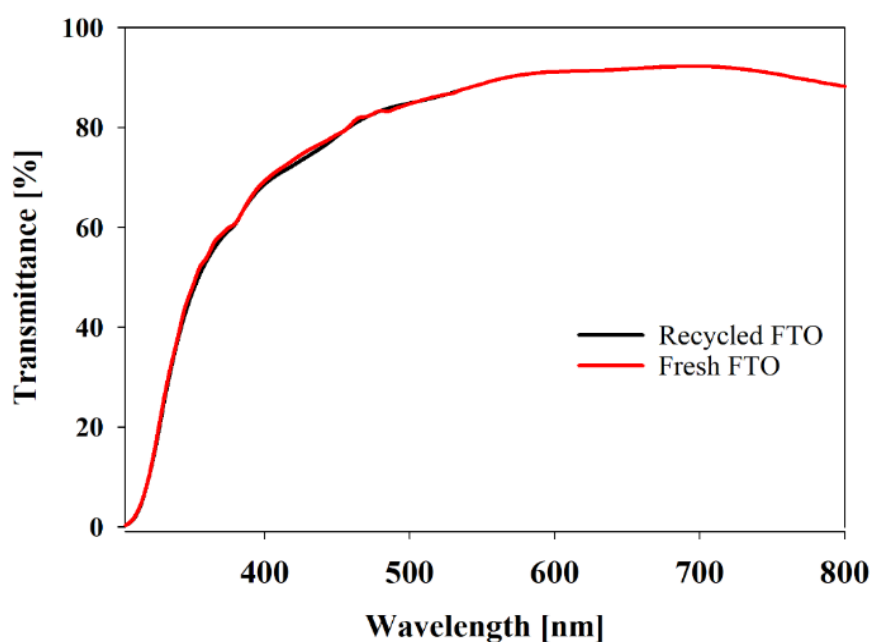


Figure 4. 12 Transmittance spectra of fresh FTO and recycled FTO substrate.

#### 4.3.5. Recycled FTO electrical properties by Hall effect measurement:

Table 4. 2 Electrical properties of fresh FTO and recycled FTO.

Properties	Fresh FTO	Recycled FTO
Carrier Concentration (1/cm)	$-8 \times 10^{20}$	$-6.1 \times 10^{20}$
Mobility ( $\text{cm}^2 \text{V}^{-1} \text{s}^{-1}$ )	$2.3 \times 10^{-1}$	$2.8 \times 10^{-1}$
Resistivity ( $\Omega \text{ cm}$ )	$3.13 \times 10^{-4}$	$3.59 \times 10^{-4}$
Conductivity ( $\Omega^{-1} \text{ cm}^{-1}$ )	$3.2 \times 10^{-3}$	$2.8 \times 10^{-3}$

Hall measurements are important to directly obtain the charge carrier concentration, mobility and resistivity conductivity of a semiconductor. It has examined the electrical properties of the fresh FTO and recycled FTO substrates. Results showed that the fresh and recycled FTO have corresponding carrier concentrations of  $-8 \times 10^{20}$  1/cm and  $-6.1 \times 10^{20} \text{ cm}^2 \text{V}^{-1} \text{S}^{-1}$ , mobilities of  $2.3 \times 10^{-1}$  and  $2.8 \times 10^{-1} \text{ cm}^2 \text{V}^{-1} \text{S}^{-1}$  and conductivities of  $3.2 \times 10^{-3}$  and  $2.8 \times 10^{-3} \Omega \text{ cm}$ . The difference can be attributed to the increase in electrical resistivity due to substantial disordered states with dopant atoms not activated between crystalline grains during the electrical measurements. The resistivity of a semiconducting material, a direct function of dopant concentration, is one of the basic parameters characterising solar cell. Calculation results showed that the resistivities of the fresh and recycled FTO were  $3.13 \times 10^{-4}$  and  $2.8 \times 10^{-3} \Omega \text{ cm}$ , respectively.

#### 4.3.6. FTO morphology and roughness analysis by AFM:

The AFM image acquisition of recovered FTO using the DMF solution was challenging most probably due to the appreciable level of PSC component layer residues on the surface, which is consistent with our investigation. In contrast to this result, AFM topographic images were successfully obtained for the fresh and recycled FTO. The topographic images showed a continuous and uniform grain-like structure along the surface for all samples.



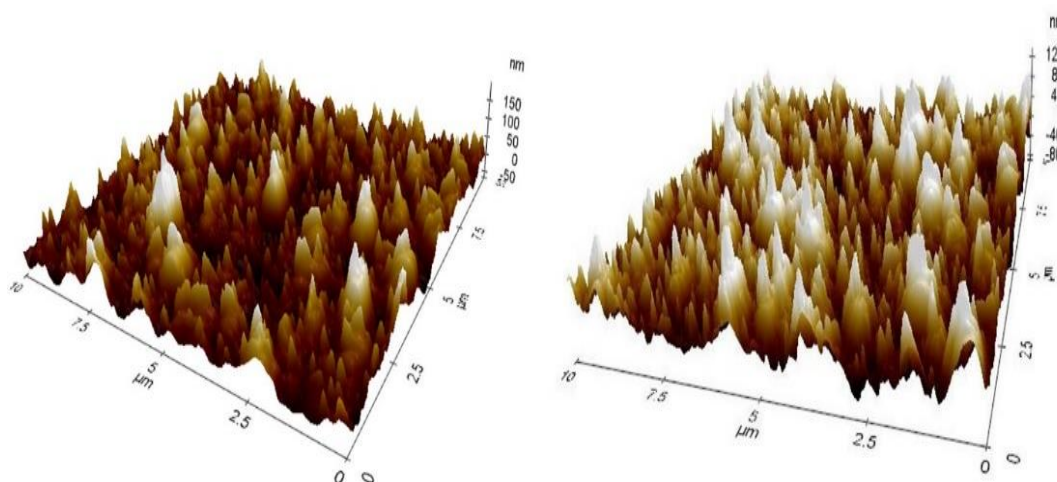


Figure 4. 13 AFM 3D top surface (a) Fresh FTO substrate (b) Recycled FTO substrate.

Table 4. 3 AFM roughness data.

Sample Name	Roughness RMS (nm)
Fresh FTO substrate	27.711
Recycled FTO substrate	27.700

RMS roughness values were obtained over  $10 \times 10 \mu\text{m}^2$  AFM topographic images. The RMS value of the recycled FTO substrate was 27.700 nm as shown in Figure 4.13. (b), which is close to that of the fresh FTO substrate (RMS 27.711 nm). Therefore, AFM image analysis clearly indicated that the proposed method to recover FTO from PSC is effective in terms of morphological and roughness aspects.

#### 4.4. Qualitatively analysis of gold by XRD measurement:

The purity of recovered gold was confirmed by XRD analysis. No trace of lead was found on the material recovered from the chlorobenzene bath (see Figure 4.14). Thus, the possibility of slight organic impurities on the surface slowing from evaporated organic HTM cannot be disregarded. The crystallinity of synthesised Au was investigated by X-ray diffraction (XRD), and corresponding XRD patterns are shown in Figure 4.14. Gold nanocrystals demonstrated four peaks at  $2\theta = 38.1^\circ$ ,  $44.3^\circ$ ,  $64.5^\circ$  and  $77.7^\circ$ . All four peaks matched the traditional Bragg reflections (111), (200),

(220) and (311) of face centred cubic lattice. The intense diffraction at 38.1 peak shows that the desired development alignment of zero valent gold was fixed in the (111) direction. Molecular-sized solids formed with a repeating 3D pattern of atoms or molecules with an equal distance between individual parts. This XRD design is characteristic of pure Au nanocrystals.

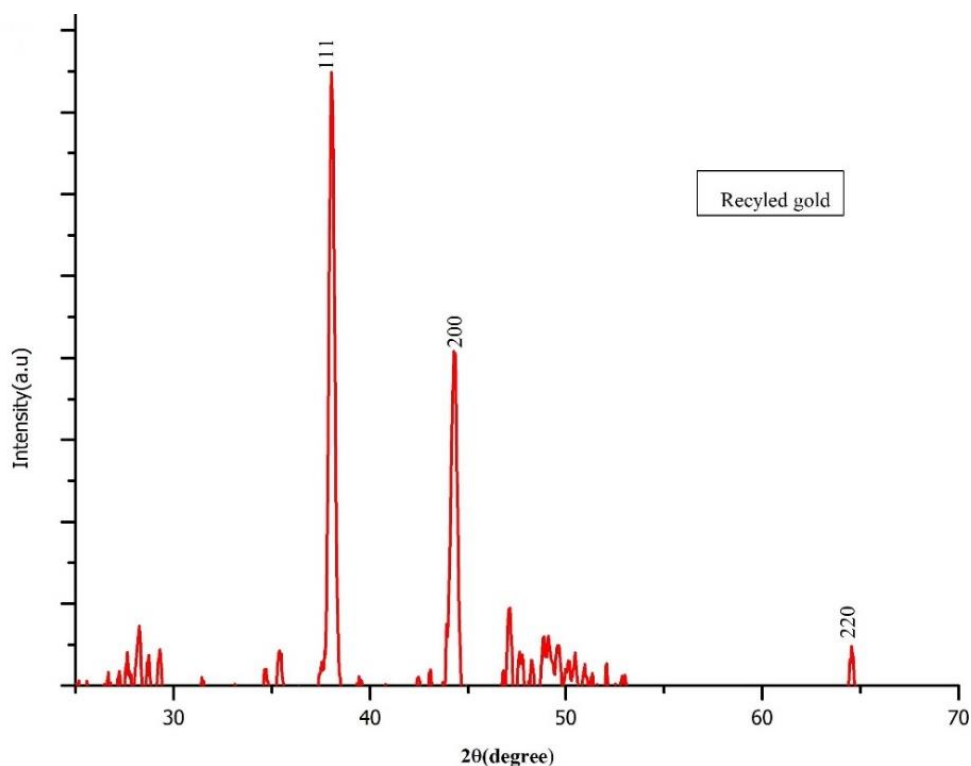


Figure 4. 14 XRD analysis for recycled gold.

#### 4.5. Recovered ITO substrate qualitative analysis by UV-vis spectroscopy:

In this part, obtained the reference and recycled ITO substrates. The transmittances of the substrate were studied by UV-vis absorption for the fresh and recycled ITO, and the results are presented in Figure 4.15. The transmittance of the recycled ITO substrate was around 80% for most visible spectrum, which is similar to that of the fresh ITO. Moreover, the electrode, HTM and absorber layer were successfully removed, as can be observed in the transmittance spectrum.

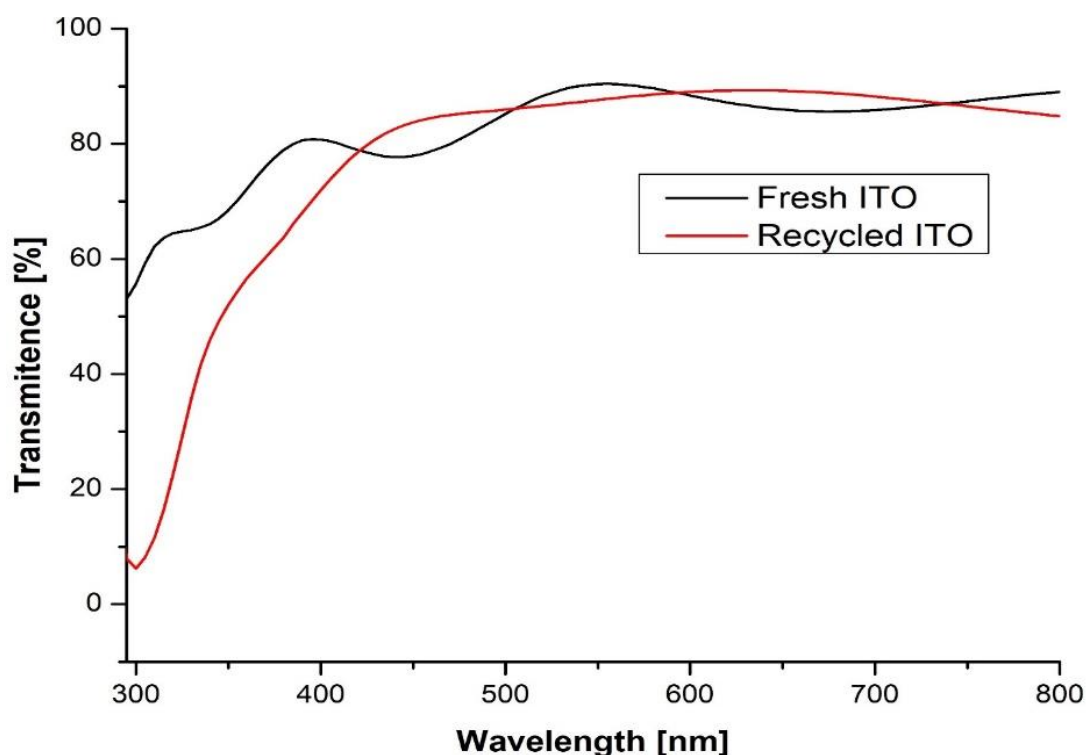


Figure 4. 15 Transmittance Spectra of Fresh ITO and Recycle ITO Substrate.

#### 4.6. Quantitative analysis by ICP-MS measurement:

According to the ICP-MS measurement, the aqua regia solution used for the trace the heavy metal. The aqua regia fraction concentrations of lead iodide and titanium were 201.65 and 13.8011  $\mu\text{g mL}^{-1}$ , respectively. Recovery rate was also quantitatively obtained, and it was comparable with the result from method 1.

This is a specific limitation of the experimental set-up in laboratory. Further research should be conducted to explain the method.

Table 4. 4 Metal concentration measured by ICP-MS.

<b>Solution</b>	<b>Pb (<math>\mu\text{g mL}^{-1}</math>)</b>	<b>Ti (<math>\mu\text{g mL}^{-1}</math>)</b>
<b>Aqua regia</b>	201.65	13.8011

#### **4.7. Lab scal recycle cost:**

In this research projected the price of the various recycled layers in a perovskite-based solar cell with planar structure. To make a reasonable correlation between the various layers, the cost of the synthetic compounds was taken for enormous lab-scale amounts from various company providers. In this budget evaluation, overlooked the solvents because their cost commitment is immaterial. The only roughly estimated the recycling process. All things considered; the assessed expenses can be utilised as a guide to determine which layers are the most encouraging to reuse from a practical perspective.

The costs of the reagents used in this experiment are as follows: 2L chlorobenzene (Sigma–Aldrich anhydrous, 99.8%), 354 USD; 12 mL solution, 2.12 USD; and 2.5L N,N-dimethylformamide (Sigma Aldrich anhydrous, 99.8%), 1.72 USD (Internet sources July 2019).

## Chapter 5

### Conclusion and References

#### Conclusion

The modern research introduced an outline of feasible PV recycling process for solar PV modules, including c-Si and thin-film technologies. The inspiration, regulation and present methods were considered, and potential problems were delivered. Recent studies have found it difficult to assess how solar PV panel recycling performance will improve in the long term, because the time frame within which recycling of solar PV materials occurs is estimated around 25 years. It is outstanding that reusing of EoL PV modules has positive impacts on the environmental effects. Reprocessing of PV modules can eliminate and preserve theoretically dangerous materials (e.g. lead, cadmium, and selenium), recover rare substrate (e.g. silver, tellurium and indium) and make them accessible for upcoming consumption.

The c-Si panels are typically processed through the physical and chemical treatment. Solar panel development for recovery wafers recycling process and re-incorporating them into new modules, had not been implemented on large scale as it was found to be cost inefficient. PV CYCLE claims breakthroughs in PV module recycling with a 96% recycling rate. CdTe panels are recycled by the many manufacturers. The recycling comprises a multi-step process; where the modules size is reduced, glass and laminate are mechanically separated, the semiconductor is removed by chemical method. The resulting metal-rich solutions are precipitated out and ultimately processed and refined. The glass cullet obtained in the process is recovered, cleaned, and re-sold. Literature shows 90% recycling of glass and 95% of the semiconductors by many researchers.

Third-generation PV perovskite solar cell has not been available in the market share today. The waste volumes are consequently small (lab scale). Meanwhile, recycling of perovskite solar cell lab-scale recycled process is compared with the 1st and 2nd generation solar cells for feasibility study. On the other hand, during treatment of c-Si and CdTe TCO substrate breaks down, however; PSCs have recovered has a minor effect on TCO substrate (lab scale).

The current study optimises perovskite solar cell with a p-i-n configuration using SCAPS simulator. TCO/CdS/Perovskite/PEDOT: PSS structure is the primary modelled solar cell. Candidate materials of 300–1000 nm absorber layer thickness and  $10^{11}$ – $10^{17}$  absorber layer defect density is obtained when energy level is 0.6 eV. Based on the simulation result, >25% PCE is obtained with  $V_{oc}$ , FF and  $J_{sc}$  as of 1.2V, 85 and  $J_{sc} > 27$  mA/cm<sup>2</sup> respectively. Increase in absorber layer thickness causes the perovskite solar cell efficiency to rapidly increase and  $V_{oc}$  decreases. Suitable absorber thickness of 400 nm < 700 nm and defect density of  $10^{11} < 10^{14}$  are found to be optimal.

The device fabricated the perovskite planar structure and characterized by the reference planar perovskite device were analysed. The typical deviations of photovoltaic factors such as PCE were 4.7% and the stability 4 hours.

The planar structure of perovskite solar cell recycled by using layer by layer process. Recycled materials and FTO substrate were characterized by using different machine. The HTM layer as Spiro-OMeTAD material recovered and ensured by the using H-NMR analysis. The hazardous heavy material Pb detected by used ICP-MS. The n- type material titanium detected by ICP-MS. Furthermore, the recovered FTO substrate obtained the electrical properties, transmittance, top surface, element percentage, chemical bond, surface roughness.

Second method is one step solution process, to recover the ITO substrate. Pb and titanium material were detected by the ICP-MS and ITO substrate obtained on transmittance. However, further research is required to make sure the ITO recovery and for material separation from the chemical solution.

## References

1. Heidari, N. and Pearce, J.M., 2016. A review of greenhouse gas emission liabilities as the value of renewable energy for mitigating lawsuits for climate change related damages. *Renewable and sustainable energy reviews*, 55, pp.899-908.
2. Strantzali, E. and Aravossis, K., 2016. Decision making in renewable energy investments: A review. *Renewable and Sustainable Energy Reviews*, 55, pp.885-898.
3. IEA International Energy Agency. (2018). Retrieved from <https://www.iea.org/>
4. Solar Power Europe, 2018. *Global Market Outlook for Solar Power 2018 - 2022*, Global Market Outlook.
5. Paiano, A., 2015. Photovoltaic waste assessment in Italy. *Renewable and Sustainable Energy Reviews*, 41, pp.99-112.
6. International Energy Agency, 2015. *Energy Technology Perspectives: Mobilising Innovation to Accelerate Climate Action 2015*.
7. Shin, J., Park, J. and Park, N., 2017. A method to recycle silicon wafer from end-of-life photovoltaic module and solar panels by using recycled silicon wafers. *Solar Energy Materials and Solar Cells*, 162, pp.1-6.
8. Xu, Y., Li, J., Tan, Q., Peters, A.L. and Yang, C., 2018. Global status of recycling waste solar panels: A review. *Waste Management*, 75, pp.450-458.
9. The International Energy Agency (IEA) - Photovoltaic Power Systems Programme - 2018 Snapshot of Global Photovoltaic Markets 1–16.
10. Sherman, R.O. and Eggenberger, T., 2008. Transitioning internationally recruited nurses into clinical settings. *The Journal of Continuing Education in Nursing*, 39(12), pp.535-544.
11. Sinke, W.C., Ballif, C., Bett, A., Dimmler, B., Dimova-Malinovska, D., Fath, P., Mason, N., Ferrazza, F., Gabler, H., Hall, M. and Martí, A., 2007. A strategic research agenda for photovoltaic solar energy technology (No. CONF).
12. Barnes, L.L., 2017. *Environmental Impact of Solar Panel Manufacturing and End-of-Life Management: Technology and Policy Options*.

13. Kojima, A., Teshima, K., Shirai, Y. and Miyasaka, T., 2009. Organometal halide perovskites as visible-light sensitizers for photovoltaic cells. *Journal of the American Chemical Society*, 131(17), pp.6050-6051.
14. Kim, J., Hou, B., Park, C., Bahn, C.B., Hoffman, J., Black, J., Bhattacharya, A., Balke, N., Hong, H., Kim, J.H. and Hong, S., 2017. Effect of defects on reaction of NiO surface with Pb-contained solution. *Scientific reports*, 7, p.44805.
15. Kearney, K., Seo, G., Matsushima, T., Adachi, C., Ertekin, E. and Rockett, A., 2018. Computational Analysis of the Interplay between Deep Level Traps and Perovskite Solar Cell Efficiency. *Journal of the American Chemical Society*, 140(46), pp.15655-15660.
16. Heo, S., Seo, G., Lee, Y., Lee, D., Seol, M., Lee, J., Park, J.B., Kim, K., Yun, D.J., Kim, Y.S. and Shin, J.K., 2017. Deep level trapped defect analysis in CH<sub>3</sub>NH<sub>3</sub>PbI<sub>3</sub> perovskite solar cells by deep level transient spectroscopy. *Energy & Environmental Science*, 10(5), pp.1128-1133.
17. Jamal, M.S., Shahahmadi, S.A., Chelvanathan, P., Alharbi, H.F., Karim, M.R., Dar, M.A., Luqman, M., Alharthi, N.H., Al-Harhi, Y.S., Aminuzzaman, M. and Asim, N., 2019. Effects of growth temperature on the photovoltaic properties of RF sputtered undoped NiO thin films. *Results in Physics*, 14, p.102360.
18. Sherkar, T.S., Momblona, C., Gil-Escrig, L., Ávila, J., Sessolo, M., Bolink, H.J. and Koster, L.J.A., 2017. Recombination in perovskite solar cells: significance of grain boundaries, interface traps, and defect ions. *ACS energy letters*, 2(5), pp.1214-1222.
19. Kim, J., Saidaminov, M.I., Tan, H., Zhao, Y., Kim, Y., Choi, J., Jo, J.W., Fan, J., Quintero-Bermudez, R., Yang, Z. and Quan, L.N., 2018. Amide-catalyzed phase-selective crystallization reduces defect density in wide-bandgap perovskites. *Advanced Materials*, 30(13), p.1706275.
20. Yu, Z., Leilaouioun, M. and Holman, Z., 2016. Selecting tandem partners for silicon solar cells. *Nat. Energy*, 1(11), p.16137.
21. McMeekin, D.P., Sadoughi, G., Rehman, W., Eperon, G.E., Saliba, M., Hörantner, M.T., Haghighirad, A., Sakai, N., Korte, L., Rech, B. and Johnston, M.B., 2016. A mixed-cation lead mixed-halide perovskite absorber for tandem solar cells. *Science*, 351(6269), pp.151-155.



22. Correa-Baena, J.P., Turren-Cruz, S.H., Tress, W., Hagfeldt, A., Aranda, C., Shooshtari, L., Bisquert, J. and Guerrero, A., 2017. Changes from bulk to surface recombination mechanisms between pristine and cycled perovskite solar cells. *ACS Energy Letters*, 2(3), pp.681-688.
23. Kim, J., Chung, C.H. and Hong, K.H., 2016. Understanding of the formation of shallow level defects from the intrinsic defects of lead tri-halide perovskites. *Physical Chemistry Chemical Physics*, 18(39), pp.27143-27147.
24. Ran, C., Xu, J., Gao, W., Huang, C. and Dou, S., 2018. Defects in metal triiodide perovskite materials towards high-performance solar cells: origin, impact, characterization, and engineering. *Chemical Society Reviews*, 47(12), pp.4581-4610.
25. Azpiroz, J.M., Mosconi, E., Bisquert, J. and De Angelis, F., 2015. Defect migration in methylammonium lead iodide and its role in perovskite solar cell operation. *Energy & Environmental Science*, 8(7), pp.2118-2127.
26. Uberuaga, B.P., Vernon, L.J., Martinez, E. and Voter, A.F., 2015. The relationship between grain boundary structure, defect mobility, and grain boundary sink efficiency. *Scientific reports*, 5, p.9095.
27. Chueh, W.C. and Haile, S.M., 2009. Electrochemical studies of capacitance in cerium oxide thin films and its relationship to anionic and electronic defect densities. *Physical Chemistry Chemical Physics*, 11(37), pp.8144-8148.
28. Macdonald, D.D., 2011. The history of the point defect model for the passive state: a brief review of film growth aspects. *Electrochimica Acta*, 56(4), pp.1761-1772.
29. IEA Photovoltaic Power Systems Programme, 2016. 2015 Snapshot of global photovoltaic markets. *Iea Pvps T1-29:2016* 1–19.
30. Irena, Iea-pvps, 2016. End-of-Life Management: Solar Photovoltaic Panels.
31. Sica, D., Malandrino, O., Supino, S., Testa, M. and Lucchetti, M.C., 2018. Management of end-of-life photovoltaic panels as a step towards a circular economy. *Renewable and Sustainable Energy Reviews*, 82, pp.2934-2945.
32. Komoto, K., Lee, J.S., Zhang, J., Ravikumar, D., Sinha, P., Wade, A. and Heath, G., 2018. End-of-Life Management of Photovoltaic Panels: Trends in PV

- Module Recycling Technologies. IEA PVPS Task 12, International Energy Agency Power Systems Programme, Report IEA-PVPS T12, 10.
33. Doi, T., Tsuda, I., Unagida, H., Murata, A., Sakuta, K. and Kurokawa, K., 2001. Experimental study on PV module recycling with organic solvent method. *Solar energy materials and solar cells*, 67(1-4), pp.397-403.
  34. Palitzsch, W. and Loser, U., 2012, June. Economic PV waste recycling solutions—Results from R&D and practice. In 2012 38th IEEE Photovoltaic Specialists Conference (pp. 000628-000631). IEEE.
  35. Klugmann-Radziemska, E. and Ostrowski, P., 2010. Chemical treatment of crystalline silicon solar cells as a method of recovering pure silicon from photovoltaic modules. *Renewable Energy*, 35(8), pp.1751-1759.
  36. Kang, S., Yoo, S., Lee, J., Boo, B. and Ryu, H., 2012. Experimental investigations for recycling of silicon and glass from waste photovoltaic modules. *Renewable Energy*, 47, pp.152-159.
  37. Orac, D., Havlik, T., Maul, A. and Berwanger, M., 2015. Acidic leaching of copper and tin from used consumer equipment. *Journal of Mining and Metallurgy B: Metallurgy*, 51(2), pp.153-161.
  38. Pagnanelli, F., Moscardini, E., Granata, G., Atia, T.A., Altimari, P., Havlik, T. and Toro, L., 2017. Physical and chemical treatment of end of life panels: an integrated automatic approach viable for different photovoltaic technologies. *Waste management*, 59, pp.422-431.
  39. Jung, B., Park, J., Seo, D. and Park, N., 2016. Sustainable system for raw-metal recovery from crystalline silicon solar panels: from noble-metal extraction to lead removal. *ACS Sustainable Chemistry & Engineering*, 4(8), pp.4079-4083.
  40. Kim, Y. and Lee, J., 2012. Dissolution of ethylene vinyl acetate in crystalline silicon PV modules using ultrasonic irradiation and organic solvent. *Solar energy materials and solar cells*, 98, pp.317-322.
  41. Marwede, M., Berger, W., Schlummer, M., Mäurer, A. and Reller, A., 2013. Recycling paths for thin-film chalcogenide photovoltaic waste—Current feasible processes. *Renewable Energy*, 55, pp.220-229.
  42. Mezei, A., Ashbury, M., Canizares, M., Molnar, R., Given, H., Meader, A., Squires, K., Ojebuoboh, F., Jones, T. and Wang, W., 2008. Hydrometallurgical

- recycling of the semiconductor material from photovoltaic materials-Part one: Leaching. Hydrometallurgy, p.209.
43. Krueger, L., 2010. First solar's module collection and recycling program. First Solar Inc. Online verfügbar unter [http://www.solarscorecard.com/panel/pdf/Lisa\\_Krueger.pdf](http://www.solarscorecard.com/panel/pdf/Lisa_Krueger.pdf)., zuletzt geprüft am, 29, p.2015.
  44. Weimann, K. and Simon, F.G., 2017. RESOLVED-Recovery of Solar Valuable Materials, Enrichment and Decontamination.
  45. Wang, W. and Fthenakis, V., 2005. Kinetics study on separation of cadmium from tellurium in acidic solution media using ion-exchange resins. Journal of hazardous materials, 125(1-3), pp.80-88.
  46. Fthenakis, V.M. and Wang, W., 2006. Extraction and separation of Cd and Te from cadmium telluride photovoltaic manufacturing scrap. Progress in Photovoltaics: Research and Applications, 14(4), pp.363-371.
  47. Wang, W. and Fthenakis, V., 2005. Kinetics study on separation of cadmium from tellurium in acidic solution media using ion-exchange resins. Journal of hazardous materials, 125(1-3), pp.80-88.
  48. Fthenakis, V. and Furey, M., 2013. Life Cycle Analysis and Recycling of CdTe Solar Modules (No. BNL-101221-2013-CRAD). Brookhaven National Laboratory (BNL), Upton, NY (United States).
  49. Dattilo, M., 2011, February. CI (G) S PV modules: recycling technology status. In 2nd International Conference on PV Module Recycling (Vol. 25).
  50. Latunussa, C.E., Ardente, F., Blengini, G.A. and Mancini, L., 2016. Life Cycle Assessment of an innovative recycling process for crystalline silicon photovoltaic panels. Solar energy materials and solar cells, 156, pp.101-111.
  51. Tao, J. and Yu, S., 2015. Review on feasible recycling pathways and technologies of solar photovoltaic modules. Solar energy materials and solar cells, 141, pp.108-124.
  52. Wang, T.Y., Hsiao, J.C. and Du, C.H., 2012, June. Recycling of materials from silicon base solar cell module. In 2012 38th IEEE Photovoltaic Specialists Conference (pp. 002355-002358). IEEE.

53. Doni, A. and Dughiero, F., 2012, June. Electrothermal heating process applied to c-Si PV recycling. In 2012 38th IEEE Photovoltaic Specialists Conference (pp. 000757-000762). IEEE.
54. Granata, G., Pagnanelli, F., Moscardini, E., Havlik, T. and Toro, L.J.S.E.M., 2014. Recycling of photovoltaic panels by physical operations. *Solar energy materials and solar cells*, 123, pp.239-248.
55. Berger, W., Simon, F.G., Weimann, K. and Alsema, E.A., 2010. A novel approach for the recycling of thin film photovoltaic modules. *Resources, Conservation and Recycling*, 54(10), pp.711-718.
56. Palitzsch, W. and Loser, U., 2013. Systematic photovoltaic waste recycling. *Green*, 3(1), pp.79-82.
57. McDonald, N.C. and Pearce, J.M., 2010. Producer responsibility and recycling solar photovoltaic modules. *Energy Policy*, 38(11), pp.7041-7047.
58. Bruton, T.M., 1994. Re-cycling of high value, high energy content components of silicon PV modules. In *Proc. of 12th EC-PVSEC* (pp. 303-304).
59. Ding, M., Xu, Z., Wang, W., Wang, X., Song, Y. and Chen, D., 2016. A review on China' s large-scale PV integration: Progress, challenges and recommendations. *Renewable and Sustainable Energy Reviews*, 53, pp.639-652.
60. Eberspacher, C. and Fthenakis, V.M., 1997, January. Disposal and recycling of end-of-life PV modules. In *Conference Record of the Twenty Sixth IEEE Photovoltaic Specialists Conference-1997* (pp. 1067-1072). IEEE.
61. Fthenakis, V.M., 2000. End-of-life management and recycling of PV modules. *Energy Policy*, 28(14), pp.1051-1058.
62. Fthenakis, V.M., Kim, H.C. and Alsema, E., 2008. Emissions from photovoltaic life cycles. *Environmental science & technology*, 42(6), pp.2168-2174.
63. Schnoor, J.L., 2012. Extended producer responsibility for e-waste.
64. Cucchiella, F. and Rosa, P., 2015. End-of-Life of used photovoltaic modules: A financial analysis. *Renewable and Sustainable Energy Reviews*, 47, pp.552-561.

65. Wessendorf, C.D., Hanisch, J., Müller, D. and Ahlswede, E., 2018. CdS as Electron Transport Layer for Low-Hysteresis Perovskite Solar Cells. *Solar RRL*, 2(5), p.1800056.
66. Mandadapu, U., Vedanayakam, S.V. and Thyagarajan, K., 2017. Simulation and analysis of lead based perovskite solar cell using SCAPS-1D. *Indian J. Sci. Technol*, 10, pp.1-8.
67. Huang, S., Rui, Z., Chi, D. and Bao, D., 2019. Influence of defect states on the performances of planar tin halide perovskite solar cells. *Journal of Semiconductors*, 40(3), p.032201.
68. Kim, H.P., bin Mohd Yusoff, A.R. and Jang, J., 2019. Polystyrene enhanced crystallization of perovskites towards high performance solar cells. *Nanoscale Advances*, 1(1), pp.76-85.
69. Singh, R., Singh, P.K., Bhattacharya, B. and Rhee, H.W., 2019. Review of current progress in inorganic hole-transport materials for perovskite solar cells. *Applied Materials Today*, 14, pp.175-200.
70. Jamal, M.S., Shahahmadi, S.A., Chelvanathan, P., Asim, N., Misran, H., Hossain, M.I., Amin, N., Sopian, K. and Akhtaruzzaman, M., 2019. Effect of defect density and energy level mismatch on the performance of perovskite solar cells by numerical simulation. *Optik*, 182, pp.1204-1210.
71. Sobayel, K., Akhtaruzzaman, M., Rahman, K.S., Ferdaous, M.T., Al-Mutairi, Z.A., Alharbi, H.F., Alharthi, N.H., Karim, M.R., Hasmady, S. and Amin, N., 2019. A comprehensive defect study of tungsten disulfide (WS<sub>2</sub>) as electron transport layer in perovskite solar cells by numerical simulation. *Results in Physics*, 12, pp.1097-1103.
72. Giorgi, G., Fujisawa, J.I., Segawa, H. and Yamashita, K., 2013. Small photocarrier effective masses featuring ambipolar transport in methylammonium lead iodide perovskite: a density functional analysis. *The journal of physical chemistry letters*, 4(24), pp.4213-4216.
73. Konstantakou, M. and Stergiopoulos, T., 2017. A critical review on tin halide perovskite solar cells. *Journal of Materials Chemistry A*, 5(23), pp.11518-11549.

74. Ngoupo, A.T., Ouédraogo, S. and Ndjaka, J.M., 2019. Numerical analysis of interface properties effects in CdTe/CdS: O thin film solar cell by SCAPS-1D. *Indian Journal of Physics*, pp.1-13.
75. Azri, F., Meftah, A., Sengouga, N. and Meftah, A., 2019. Electron and hole transport layers optimization by numerical simulation of a perovskite solar cell. *Solar Energy*, 181, pp.372-378.
76. Homes, C.C., Vogt, T., Shapiro, S.M., Wakimoto, S. and Ramirez, A.P., 2001. Optical response of high-dielectric-constant perovskite-related oxide. *Science*, 293(5530), pp.673-676.
77. Wehrenfennig, C., Eperon, G.E., Johnston, M.B., Snaith, H.J. and Herz, L.M., 2014. High charge carrier mobilities and lifetimes in organolead trihalide perovskites. *Advanced materials*, 26(10), pp.1584-1589.
78. Ferdaous, M.T., Shahahmadi, S.A., Chelvanathan, P., Akhtaruzzaman, M., Alharbi, F.H., Sopian, K., Tiong, S.K. and Amin, N., 2019. Elucidating the role of interfacial MoS<sub>2</sub> layer in Cu<sub>2</sub>ZnSnS<sub>4</sub> thin film solar cells by numerical analysis. *Solar Energy*, 178, pp.162-172.
79. Gu, Z., Chen, F., Zhang, X., Liu, Y., Fan, C., Wu, G., Li, H. and Chen, H., 2015. Novel planar heterostructure perovskite solar cells with CdS nanorods array as electron transport layer. *Solar Energy Materials and Solar Cells*, 140, pp.396-404.
80. Karimi, E. and Ghorashi, S.M.B., 2017. Investigation of the influence of different hole-transporting materials on the performance of perovskite solar cells. *Optik*, 130, pp.650-658.
81. Zuo, L., Guo, H., deQuilettes, D.W., Jariwala, S., De Marco, N., Dong, S., DeBlock, R., Ginger, D.S., Dunn, B., Wang, M. and Yang, Y., 2017. Polymer-modified halide perovskite films for efficient and stable planar heterojunction solar cells. *Science advances*, 3(8), p.e1700106.
82. Zhao, X., Liu, S., Zhang, H., Chang, S.Y., Huang, W., Zhu, B., Shen, Y., Shen, C., Wang, D., Yang, Y. and Wang, M., 2019. 20% Efficient Perovskite Solar Cells with 2D Electron Transporting Layer. *Advanced Functional Materials*, 29(4), p.1805168.

83. Snaith, H.J., 2010. Estimating the maximum attainable efficiency in dye-sensitized solar cells. *Advanced Functional Materials*, 20(1), pp.13-19.
84. Khadka, D.B., Shirai, Y., Yanagida, M. and Miyano, K., 2019. Unravelling the Impacts Induced by Organic and Inorganic Hole Transport Layers in Inverted Halide Perovskite Solar Cells. *ACS applied materials & interfaces*.
85. Zhu, L., Chen, C., Li, F., Shen, Z., Weng, Y., Huang, Q. and Wang, M., 2019. Enhancing the efficiency and stability of perovskite solar cells by incorporating CdS and Cd (SCN<sub>2</sub> H<sub>4</sub>)<sub>2</sub> Cl<sub>2</sub> into the CH<sub>3</sub> NH<sub>3</sub> PbI<sub>3</sub> active layer. *Journal of Materials Chemistry A*, 7(3), pp.1124-1137.

## VITAE

**Name** Mr. Md. Shahariar Chowdhury

**Student ID** 6010920007

### **Educational Attainment**

Degree	Name of Institution	Year of Graduation
Bachelor of Science in Electrical and Electronic Engineering	Atish Dipankar University Science and Technology, Bangladesh	2016

### **Scholarship Awards during Enrolment**

1. The scholarship awards of Thailand's Education Hub for Southern Region of ASEAN Countries (TEH-AC) (Contract No.: THE-AC 06212017), funds for Master of Science program from the graduate school, Prince of Songkla University, Hat Yai, Thailand.
2. Research Development Fund for Quality Graduate Level Research.
3. Graduate School Dissertation Funding for thesis, Prince of Songkla University.

### **Work – Position and Address**

- Asst. Engineer at Biswas Builders Limited. Dhaka Bangladesh.